exchange Hamiltonian. We show the temperature dependence of $1-u-w$ and $1-u-v$ for the case of $S=2$ in Fig. 2.[10] As noted by Bloch,[5] two roots are found for $\alpha'(T)$, which is equal to $1-u-w$ in the present paper, in the range of temperature 0°K–$T_M'$. One of these roots, which is denoted by the solid line, corresponds in the low-temperature limit to the standard results of the spin-wave theory, and the other, which is denoted by the dashed line, corresponds to a dubious solution. As can be seen in Fig. 2, $1-u-v$ corresponding to the standard solution is positive in the temperature range 0°K–$T_0$ and it is negative for $T_0<T<T_M'$. On the other hand, $1-u-v$ corresponding to the dubious solution is always negative in the temperature range 0°K–$T_M'$. This shows that the solutions obtained for finite values of $\theta$ correspond to the standard solutions. We show $T_0$ in the case of the exchange Hamiltonian in Table III for several values of $S$. If the exchange Hamiltonian is considered as the limit of the present Hamiltonian for an infinitesimal anisotropy, the maximum temperature will not be given by $T_M'$ but by $T_0$.

[10] The self-consistent solution for the case of the exchange Hamiltonian, which is shown in Fig. 2 and Table III, was obtained by solving Eq. (17c). We also solved Eqs. (16a) and (16b), in which $\theta$ was replaced by zero, by use of the iterative method described in Ref. 8. The latter method is found to be useful only below $T_0$, because the convergence of $v_n$ and $w_n$ in the iterative treatment is very poor above this temperature.

## ACKNOWLEDGMENTS

The author wishes to express his sincere thanks to Professor Tomoyasu Tanaka for his numerous enlightening discussions. The author also would like to thank Professor Junjiro Kanamori of Osaka University for his valuable discussions in the initial stage of this work. He is also much indebted to N. L. Bonavito for his help with numerical computations and for improving the manuscript.

PHYSICAL REVIEW VOLUME 180, NUMBER 2 10 APRIL 1969

# Magnon Sidebands in the Optical Absorption Spectrum of $MnF_2$†

RICHARD S. MELTZER*
*James Franck Institute and Department of Chemistry, University of Chicago, Chicago, Illinois 60637*

AND

MARIAN LOWE‡ AND DONALD S. MCCLURE
*Department of Chemistry, Princeton University, Princeton, New Jersey 08540*

(Received 15 November 1968; revised manuscript received 19 March 1969)

The magnon sidebands and other structure in the optical spectrum of antiferromagnetic $MnF_2$ have been studied under various conditions of magnetic fields, uniaxial stress, and temperature. We present the results of such experiments for the $^4T_1$(I), $^4A_1$, $^4E$(I), $^4T_2$(II), $^4T_1$(II), and $^4E$(II) states of $Mn^{++}$ in $MnF_2$. The magnon sideband shapes have been fitted as well as possible by density-of-states calculations in which the normal magnon dispersion and an adjustable exciton dispersion were used. It has been possible in this way to identify and give the magnitude of the pair moment for the principal exchange mechanism responsible for each sideband absorption, and to give the exciton parameters for the best fit. The discrepancies in this fitting process are probably ascribable to exciton-magnon binding, and indeed one line appears to represent a bound state of an exciton and a magnon.

## I. INTRODUCTION

In the past few years there has been great interest in the optical absorption spectrum of $MnF_2$ and several other compounds which are antiferromagnetic at low temperatures. This interest has arisen because of the observation of spin-wave sidebands accompanying the pure electronic excitations of the crystal. A spin-wave sideband in the optical absorption spectrum arises from the coupling of a spin deviation (magnon) to an electronic excitation of the ions in the crystal (exciton).

The first magnon sideband identification was made by Greene *et al.*[1] in the absorption to the $^4T_1$(I) state of $MnF_2$. Since then, both the absorption and emission of this transition have been the subject of several investigations including the effects of magnetic field and uniaxial stress.[2–5] A review of this work has been given by

† Work supported by the U. S. Office of Naval Research and the National Science Foundation with equipment grants from the Advanced Research Projects Agency (at the University of Chicago).

* Present address: Department of Physics, The Johns Hopkins University, Baltimore, Md.

‡ Present address: Department of Chemistry, Boston University, Boston Mass.

[1] R. L. Greene, D. D. Sell, W. M. Yen, and A. L. Schawlow, Phys. Rev. Letters **15**, 656 (1965).

[2] D. D. Sell, R. L. Greene, and R. M. White, Phys. Rev. **158**, 489 (1967).

[3] P. G. Russell, D. S. McClure, and J. W. Stout, Phys. Rev. Letters **16**, 176 (1966).

[4] R. E. Deitz, A. Misetich, and H. J. Guggenheim, Phys. Rev. Letters **16**, 841 (1966).

[5] A. Misetich, R. E. Dietz, and H. J. Guggenheim, *Localized Excitations in Solids* (Plenum Press, Inc., New York, 1968), p. 379.

Sell.[6] Recently, magnon sidebands have been suggested as the cause of absorption in several other materials.[7–11]

We thought it important to examine carefully the sidebands of several excited states in a single material in order to examine the following four points: First, does the existing theory for magnon sideband absorption developed by Tanabe *et al.*,[12,13] Sell *et al.*,[2] and Loudon[14] apply more generally than to the sidebands of the $^4T_1$(I) state, the only case to which it has been applied in detail? Even in this case there are serious difficulties in the explanation of the line shapes of the sidebands. Secondly, we wish to examine the exciton dispersion in a series of excited states. The requirement for conservation of the **k** vector in the absorption or emission process enables one to determine the exciton dispersion by utilizing the known magnon dispersion. Thirdly, we want to obtain information about the magnitude of the exciton-magnon interaction. Finally, we wish to determine the intensity mechanism responsible for the major portion of the absorption contained in the relatively broad envelopes which accompany the exciton and sideband transitions. Are they phonon- or spin-assisted?

$MnF_2$ is a particularly suitable antiferromagnetic material to study with regard to the above objects. It has an absorption spectrum which contains a wealth of structure at low temperatures, its cubic field states are well separated in energy and easily identifiable, its ground state is simple, and its magnon dispersion has been thoroughly studied. In a previous paper we have examined in detail the single-ion pure electronic transitions of $MnF_2$.[15] We now examine the sidebands to these transitions.

In Sec. II we summarize the relevant existing theory and selection rules for magnon sidebands, presenting a few additional necessary expressions for the transition moments. We consider, in addition to the temperature-independent sideband absorption, that absorption which arises from the thermal population of magnons in the ground electronic state, which we term "hot bands." These bands were first observed in $MnF_2$ by Stout and Reed.[16] In Sec. III, we describe the experimental techniques utilized in this study. In Sec. IV we describe, in detail, the experimental results and apply the theory of Sec. II to their analysis. Finally, in Sec. V we attempt to answer the four questions posed above, which stimulated this investigation.

## II. THEORY

### A. Absorption Coefficients

The theory of the magnon sideband absorption in rutile-type antiferromagnets has been developed by several authors.[2,12–14,17] Selection rules have been derived in a general way from a knowledge of the crystal spacegroup symmetry by Sell *et al.*[2] and by Loudon.[14] Selection rules have also been given by Tanabe and Gondaira[13] based on transformation properties of the wave functions of the particular type of single-ion states being considered.

The selection rules are independent of the particular coupling mechanism giving rise to the magnon-induced transitions. However, the line shape will depend on the details of the interaction. Two different mechanisms have thus far been proposed for the magnon-exciton bands, both of which are special cases of Dexter's[18] theoretical treatment of electric dipole processes in which pairs of ions undergo simultaneous transitions. The first type involves multipole expansion of the Coulomb interaction between pairs of ions and gives the interaction between the electric dipole moment of one and the spin-orbit-induced quadrupole moment of the other as the lowest-order nonvanishing term.[17] The second type of mechanism is derived from off-diagonal exchange terms arising from the Coulomb interaction.[12] This type of mechanism is expected to be of much shorter range than the direct interaction. Experimental evidence suggests that the exchange mechanism predominates in $MnF_2$.[3,19]

Expressions for the line shapes expected in absorption when coupling is only to first and second nearest neighbors have been given in part by the authors mentioned above. For the intrinsic emission from the lowest exciton of the $^4T_1$(I) state, the line shape including the first- and second-neighbor coupling has been given by Misetich *et al.*[5] We summarize these results below and, in addition, give expressions for contributions which may arise from third-nearest-neighbor coupling.

The Hamiltonian for the crystal in an electric field may be written

$$H=H_0+V+\mathbf{E}\cdot\mathbf{P}, \tag{1}$$

where $H_0$ and **P** contain, respectively, the single-ion Hamiltonians and the electric dipole operators of all the electrons, and $V$ is the interion Coulomb interaction. Perturbation theory then leads to an effective Hamiltonian of the two-center interaction for the crystal

[6] D. D. Sell, J. Appl. Phys. **39**, 1030 (1968).
[7] R. Stevenson, Can. J. Phys. **44**, 3269 (1966).
[8] R. Stevenson, Phys. Rev. **152**, 531 (1966).
[9] V. V. Eremenko, Yu. A. Popkov, V. P. Novikov, and A. I. Belyaeva, Zh. Eksperim. i Teor. Fiz. **52**, 454 (1967) [English transl.: Soviet Phys.—JETP **25**, 297 (1967)].
[10] R. J. Elliott, M. F. Thorpe, G. F. Imbusch, R. Loudon, and J. B. Parkinson, Phys. Rev. Letters **21**, 147 (1968).
[11] K. Hoyaga, J. Phys. Soc. Japan **22**, 156 (1967).
[12] Y. Tanabe, T. Moriya, and S. Sugano, Phys. Rev. Letters **15**, 1023 (1965).
[13] Y. Tanabe and K. Gondaira, J. Phys. Soc. Japan **22**, 573 (1967).
[14] R. Loudon, Advan. Phys. **17**, 243 (1968).
[15] R. S. Meltzer and L. L. Lohr, J. Chem. Phys. **49**, 541 (1968).
[16] J. W. Stout and S. A. Reed (unpublished results).
[17] J. W. Halley and I. Silvera, Phys. Rev. Letters **15**, 664 (1965); J. W. Halley, Phys. Rev. **144**, 423 (1966).
[18] D. L. Dexter, Phys. Rev. **126**, 1962 (1962).
[19] S. J. Allen, R. Loudon, and P. L. Richards, Phys. Rev. Letters **16**, 463 (1966).

with the radiation field

$$H^{\text{ex-mag}}=\mathbf{E}\cdot(\sum_{i,j}\mathbf{P}_{ij}A_i^\dagger b_j^\dagger+\sum_{i,i'}\mathbf{P}_{ii'}A_i^\dagger a_{i'}$$
$$+\sum_{i,j}\mathbf{P}_{ij}{}^*A_i b_j+\sum_{i,i'}\mathbf{P}_{ii'}{}^*A_i a_{i'}{}^\dagger$$
$$+\text{terms for other sublattice}), \quad (2)$$

where $A_i^\dagger$ is the creation operator for a single-ion excited state on one sublattice, $b_j^\dagger$ is a creation operator for a spin deviation on the opposite sublattice, and $a_i^\dagger$ is a creation operator for a spin deviation on the same sublattice. We have included only those terms which arise from the exchange mechanism. General expressions for the $P$'s are obtained from Dexter's theory and have been given previously.[2] The Hamiltonian contains all of the terms which can lead to single-magnon sidebands. We have written only those terms which involve an excited state on sublattice $A$. The extension to sublattice $B$ is obvious. As a result of the lack of intersublattice coupling for the pure exciton,[2] the exciton is primarily on one sublattice. Therefore, of the four possible exciton symmetries at the $\Gamma$ point of the Brillouin zone, we find that the $\Gamma_1^+$ and $\Gamma_2^+$ representations and the $\Gamma_3^+$ and $\Gamma_4^+$ representations are degenerate and may be considered together. $H^{\text{ex-mag}}$ is now rewritten in terms of magnon variables and one-sublattice excitons as

$$H^{\text{ex-mag}}=\mathbf{E}\cdot\{[\mathbf{P}_0(\mathbf{k})u_\mathbf{k}+\mathbf{P}_s(\mathbf{k})v_\mathbf{k}]A_\mathbf{k}^\dagger\beta_{-\mathbf{k}}^\dagger$$
$$+[\mathbf{P}_0{}^*(\mathbf{k})u_\mathbf{k}+\mathbf{P}_s{}^*(\mathbf{k})v_\mathbf{k}]A_\mathbf{k}\beta_{-\mathbf{k}}+[\mathbf{P}_s(\mathbf{k})u_\mathbf{k}+\mathbf{P}_0(\mathbf{k})v_\mathbf{k}]$$
$$\times A_\mathbf{k}^\dagger\alpha_\mathbf{k}+[\mathbf{P}_s{}^*(\mathbf{k})u_\mathbf{k}+\mathbf{P}_0{}^*(\mathbf{k})v_\mathbf{k}]A_\mathbf{k}\alpha_\mathbf{k}^\dagger$$
$$+\text{terms for other sublattice}\}, \quad (3)$$

where

$$A_i^\dagger=N^{-1/2}\sum_\mathbf{k}e^{-i\mathbf{k}\cdot\mathbf{r}_i}A_\mathbf{k}^\dagger,$$
$$a_i^\dagger=N^{-1/2}\sum_\mathbf{k}e^{-i\mathbf{k}\cdot\mathbf{r}_i}a_\mathbf{k}^\dagger,$$
$$b_i^\dagger=N^{-1/2}\sum_\mathbf{k}e^{-i\mathbf{k}\cdot\mathbf{r}_i}b_\mathbf{k}^\dagger,$$
$$\mathbf{P}_0(\mathbf{k})=\sum_j P_{ij}e^{i\mathbf{k}\cdot(\mathbf{r}_i-\mathbf{r}_j)},$$

and

$$\mathbf{P}_s(\mathbf{k})=\sum_{i'}P_{ii'}e^{i\mathbf{k}\cdot(\mathbf{r}_i-\mathbf{r}_{i'})},$$

and $\alpha_\mathbf{k}^\dagger$ and $\beta_{-\mathbf{k}}^\dagger$ are the operators which diagonalize the magnon Hamiltonian (see Kittel[20]):

$$\alpha_\mathbf{k}^\dagger=u_\mathbf{k}a_\mathbf{k}^\dagger-v_\mathbf{k}b_{-\mathbf{k}},$$
$$\beta_\mathbf{k}^\dagger=u_\mathbf{k}b_\mathbf{k}^\dagger-v_\mathbf{k}a_{-\mathbf{k}}. \quad (4)$$

The coefficients $u_\mathbf{k}$ and $v_\mathbf{k}$ are real and satisfy $u_\mathbf{k}^2-v_\mathbf{k}^2=1$. It is important to note that $v_\mathbf{k}=0$ at the zone boundary.

[20] C. Kittel, *Quantum Theory of Solids* (John Wiley & Sons, Inc., New York, 1963).

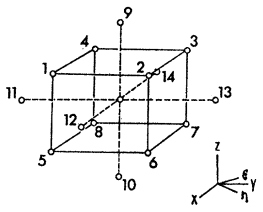


FIG. 1. Near neighbors on the same and opposite sublattices. Sites 1–8 are second nearest neighbors, sites 9 and 10 are first nearest neighbors, and sites 11–14 are third nearest neighbors.

Those terms involving the destruction of a magnon can only be active above temperatures at which magnons are thermally populated. Since the coefficient of the terms $A_\mathbf{k}^\dagger\beta_{-\mathbf{k}}^\dagger$ and $A_\mathbf{k}\beta_{-\mathbf{k}}$ and of the terms $A_\mathbf{k}^\dagger\alpha_\mathbf{k}$ and $A_\mathbf{k}\alpha_\mathbf{k}^\dagger$ are complex conjugates, the temperature-independent ("cold-band") term in absorption corresponds to the temperature-dependent ("hot-band") term in emission and vice versa.

If we now restrict the sums to first, second, and third neighbors (assuming the short-range coupling of Tanabe *et al.*), we may write the Hamiltonian as

$$H^{\text{ex-mag}}=\mathbf{E}\cdot\{[\mathbf{P}_2(\mathbf{k})u_\mathbf{k}+(\mathbf{P}_1(\mathbf{k})+\mathbf{P}_3(\mathbf{k}))v_\mathbf{k}]A_\mathbf{k}^\dagger\beta_{-\mathbf{k}}^\dagger$$
$$+[\mathbf{P}_2{}^*(\mathbf{k})u_\mathbf{k}+(\mathbf{P}_1{}^*(\mathbf{k})+\mathbf{P}_3{}^*(\mathbf{k}))v_\mathbf{k}]A_k\beta_{-k}$$
$$+[(\mathbf{P}_1(\mathbf{k})+\mathbf{P}_3(\mathbf{k}))u_\mathbf{k}+\mathbf{P}_2(\mathbf{k})v_\mathbf{k}]A_\mathbf{k}^\dagger\alpha_\mathbf{k}$$
$$+[(\mathbf{P}_1{}^*(\mathbf{k})+\mathbf{P}_3{}^*(\mathbf{k}))u_\mathbf{k}+\mathbf{P}_2{}^*(\mathbf{k})v_\mathbf{k}]A_\mathbf{k}\alpha_\mathbf{k}^\dagger$$
$$+\text{terms from other sublattice}\},$$

where $\mathbf{P}_n(k)$ gives the coupling to the $n$th nearest neighbor and, for example, $\mathbf{P}_2(\mathbf{k})=\sum_q\mathbf{P}_{0q}e^{i\mathbf{k}\cdot(\mathbf{r}_0-\mathbf{r}_q)}$, with $q$ numbering, in this example, the eight equivalent second neighbors.

The symmetry relations among the pair transition moments are found by standard group-theoretical methods and give the following expressions for the transition moments for cold-band absorption and hot-band emission:

$$M_k{}^m(\Gamma)=4i\sin\tfrac{1}{2}k_zc\,[P_1{}^m\cos\tfrac{1}{2}(k_x-k_y)a$$
$$+P_2{}^m\cos\tfrac{1}{2}(k_x+k_y)a]u_k+2iP_9{}^m(\sin k_zc)v_k,$$
$$M_k{}^l(\Gamma)=4i\cos\tfrac{1}{2}k_zc[P_1{}^l\sin\tfrac{1}{2}(k_x-k_y)a \quad (5)$$
$$-P_2{}^l\sin\tfrac{1}{2}(k_x+k_y)a]u_k$$
$$-2i[P_{11}{}^l\sin k_ya+P_{11}{}^{l*}\sin k_xa]v_k.$$

When $\Gamma=\Gamma_1^+$, $\Gamma_2^+$, then $m$ is $\xi$ and $\eta$, and $l$ is $z$. When $\Gamma=\Gamma_3^+$, $\Gamma_4^+$, then $m$ is $z$ and $l$ is $\xi$ and $\eta$. The $P_n$'s are the pair transition moments for the pair 0-$n$. The relevant $Mn^{+2}$ neighbors to ion 0 (the electronic excitation resides on ion 0) are shown in Fig. 1. To obtain the transition moments for the second sublattice, interchange $\xi$ and $\eta$, the subscripts 1 and 2, and the complex conjugation in the last term. The transition moments for hot-band absorption and cold-band emission may also be obtained from these expressions by interchanging $u_\mathbf{k}$ and $v_k$ and taking the complex conjugate of the $P_n{}^{l}$s.

Expressions for the sideband absorption coefficients depend upon the combined exciton-magnon density of states, the transition moments, and, for any hot-band

process, the magnon occupation number $\langle n_k^{\rm mag}(T)\rangle$. If we assume an independent particle model to describe the total energy of the two excitations, the combined exciton-magnon dispersion relation is

$$E_k = E_k^{\rm ex} \pm E_k^{\rm mag}. \tag{6}$$

The upper and lower signs refer to the cold-band and hot-band absorption, respectively. The negative sign reflects the fact that the magnon is being destroyed.

The resulting expressions for the absorption coefficients for the cold bands and hot bands, respectively, are[2]

$$\alpha_{\bar\nu}^{l,m}(c) = C\sum_k\sum_i |M_{ik}^{l,m}(\Gamma)|^2\delta(h\bar\nu c - E_k^{\rm ex} - E_k^{\rm mag}),$$
$$\alpha_{\bar\nu}^{l,m}(H) = C\sum_k\sum_i |M_{ik}^{l,m}(\Gamma)|^2 \times\langle n_k^{\rm mag}(T)\rangle\delta(h\bar\nu c - E_k^{\rm ex} - E_k^{\rm mag}), \tag{7}$$

where

$$C = \frac{(2\pi)^3\bar\nu}{hcnV}\left(\frac{E_{\rm eff}}{E_0}\right)^2,$$

$n$ is the refractive index, $E_{\rm eff}/E_0$ is the effective field correction, and $i$ refers to the two sublattices. The squares of the transition moments in the above expressions, summed over the two sublattices, are

$$|M_k^{l}(\Gamma)|^2 = \pi_X^{l} u_k^2 \sin^2(\tfrac{1}{2}k_x a)\cos^2(\tfrac{1}{2}k_y a)\cos^2(\tfrac{1}{2}k_z c) + \pi_3^{l} v_k^2(\sin^2 k_x a + \sin^2 k_y a), \tag{8}$$
$$|M_k^{m}(\Gamma)|^2 = u_k^2[\pi_Z^{m}\cos^2(\tfrac{1}{2}k_x a)\cos^2(\tfrac{1}{2}k_y a)\sin^2(\tfrac{1}{2}k_z c) + \pi_A^{m}\sin^2(\tfrac{1}{2}k_x a)\sin^2(\tfrac{1}{2}k_y a)\sin^2(\tfrac{1}{2}k_z c)] + \pi_1^{m} v_k^2\sin^2 k_z c.$$

We have excluded in the above all terms which are of odd power in the trigonometric functions, since they will vanish when summed over $\mathbf{k}$ space. When $\Gamma=\Gamma_1^+$, $\Gamma_2^+$, the parameters are the following function of the pair transition moments:

$$\begin{aligned}
\pi_X^{\pi} &= 64(|P_1^z|^2 + |P_2^z|^2),\\
\pi_Z^{\sigma} &= 16(|P_1^\xi + P_2^\xi|^2 + |P_1^\eta + P_2^\eta|^2),\\
\pi_A^{\sigma} &= 16(|P_1^\xi - P_2^\xi|^2 + |P_1^\eta - P_2^\eta|^2),\\
\pi_3^{\pi} &= 8|P_{11}^z|^2,\\
\pi_1^{\sigma} &= 4(|P_9^\xi|^2 + |P_9^\eta|^2);
\end{aligned} \tag{9}$$

when $\Gamma=\Gamma_3^+$, $\Gamma_4^+$,

$$\begin{aligned}
\pi_X^{\sigma} &= 32(|P_1^\xi|^2 + |P_2^\xi|^2 + |P_1^\eta|^2 + |P_2^\eta|^2),\\
\pi_Z^{\pi} &= 32|P_1^z + P_2^z|^2,\\
\pi_A^{\pi} &= 32|P_1^z - P_2^z|^2,\\
\pi_3^{\sigma} &= 4(|P_{11}^\xi|^2 + |P_{11}^\eta|^2),\\
\pi_1^{\pi} &= 8|P_9^z|^2.
\end{aligned} \tag{10}$$

The selection rules for the symmetry points in the Brillouin zone determine whether or not the corresponding critical point in the density-of-states appears as a sharp feature of the line or is quenched by the transition moment which weights the density of states in the above expressions. It has been shown that for second-neighbor coupling only the critical points $Z$, $A$, and $X$ symmetry are allowed[2,14] and the polarizations to which they contribute are determined by the exciton symmetry. The transition moments given in Eq. (8) are consistent with these selection rules and we see that the $Z$ and $A$ points contribute to one polarization, while the $X$ points contributes to the opposite polarization. We also see from these expressions that for first-nearest-neighbor coupling we expect sidebands to the $\Gamma_1^+$, $\Gamma_2^+$ excitons to appear in the $\sigma$ polarization and sidebands to the $\Gamma_3^+$, $\Gamma_4^+$ excitons in $\pi$, i.e., the same polarization as the magnetic dipole origins. For third-neighbor coupling, the sidebands will appear in the opposite polarization from that of the magnetic dipole origins. The selection rules for these three kinds of coupling are summarized in Table I. They depend solely on the neighbors coupled and not on the kind of sideband being observed.

In general, we expect absorption intensity to arise predominately from those terms which contain $u_k^2$. Terms which contain $v_k^2$ suppress the contribution of zone boundary points of the Brillouin zone where the density of states is high. Hence cold-band absorption and hot-band emission should arise from intersublattice coupling, whereas hot-band absorption and cold-band emission should result from intrasublattice first- and third-nearest-neighbor coupling terms, of which we expect the first-neighbor coupling to predominate.

### B. Magnon and Exciton Dispersion

The magnon energy dispersion for 0°K (which appears in the absorption coefficient expressions) is given by

$$E_k^{\rm mag} = 2SZ_2|J_2|\cdot(1+0.073/2S) \times[(1+\epsilon_k)^2 - \gamma_k^2]^{1/2} \pm g\beta H_0, \tag{11}$$

where $z_i$ is the number of the $i$th kind of neighbor, $S=\frac{5}{2}$, and the term $1+0.073/2S$ takes account of the zero-point spin deviations. The terms $\epsilon_k$ and $\gamma_k$ are given by

$$\epsilon_k = \frac{g\beta H_A}{2SZ_2|J_2|} - \frac{2Z_1J_1}{Z_2J_2}\sin^2(\tfrac{1}{2}k_z c) - \frac{Z_3J_3}{Z_2J_2} \times[\sin^2(\tfrac{1}{2}k_x a) + \sin^2(\tfrac{1}{2}k_y a)],$$
$$\gamma_k = \cos(\tfrac{1}{2}k_x a)\cos(\tfrac{1}{2}k_y a)\cos(\tfrac{1}{2}k_z c).$$

The well-known magnetic parameters for $MnF_2$ in units of $cm^{-1}$ are $J_1=0.22$,[21] $J_2=1.22$,[22] $J_3<0.035$,[21] and $g\beta H_A=0.737$.[23] Since the magnon dispersion depends on temperature, we must use in our analysis of the hot bands the renormalized dispersion relation[24]

$$E_k^{\rm mag}(T) = R_k(T)E_k^{\rm mag}, \tag{12}$$

[21] A. Okazaki, K. C. Tuberfield, and R. W. H. Stevenson, Phys. Letters 8, 9 (1964).
[22] C. Trapp and J. W. Stout, Phys. Rev. Letters 10, 157 (1963).
[23] F. M. Johnson and A. H. Nethercot, Jr., Phys. Rev. 114, 705 (1959).
[24] G. G. Low, *Inelastic Scattering of Neutrons* (International Atomic Energy Agency, Vienna, 1965), p. 453.

where the renormalization factor $R_k(T)$ is given by

$$R_k(T)=1-\frac{\alpha_k}{NS}\sum_{k'}\alpha_{k'}[(1+\epsilon_{k'})^2-\gamma_{k'}]^{1/2}\langle n_{k'}{}^{mag}(T)\rangle. \quad (13)$$

This is an implicit equation for $E_k{}^{mag}(T)$, since the magnon occupation number $\langle n_k{}^{mag}(T)\rangle$ is a function of the renormalized frequency. At 0°K, the dispersion relation leads to maxima in the density of states at 50.4 and 54.8 $cm^{-1}$ which correspond to the $X$ and $Z$ points of the Brillouin zone. ($J_3$ is assumed to be negligible.) For the intersublattice terms containing $u_k$ (i.e., second-neighbor cold-band absorption or hot-band emission), in the limit that both the exciton dispersion and energy associated with the exciton-magnon interaction are small, these points of the zone will appear as maxima in the magnon sideband absorptions. These are indicated by the numbers in parentheses in Table I. When either or both of these limits are not realized, the energy of the critical points, as they appear in the sidebands, will no longer correspond to the energies 50.4 and 54.8 $cm^{-1}$, and in fact the $X$ and $Z$ points may no longer even correspond to maxima in the combined exciton-magnon density of states.

Where the exciton dispersion is important we may write it as[2]

$$E_k{}^{ex}(\Gamma)=E^{MF}+\sum_{\langle ii'\rangle}V_{ii'}e^{i\mathbf{k}\cdot(\mathbf{r}_i-\mathbf{r}_{i'})}\pm\sum_{\langle ij\rangle}V_{ij}e^{i\mathbf{k}\cdot(\mathbf{r}_i-\mathbf{r}_j)}, \quad (14)$$

where $E^{MF}$ is the single-ion energy in a molecular field. The $V$'s are matrix elements for the exchange of the excitation between ions $i$ and $i'$ on the same sublattice or ions $i$ and $j$ on opposite sublattices. The second term is zero for a $\Gamma_3^+$, $\Gamma_4^+$ exciton and is negligible for a $\Gamma_1^+$, $\Gamma_2^+$ exciton, since intersublattice exchange for $MnF_2$ is very small. If we assume that only first- and third-nearest-neighbor intrasublattice terms are important, this expression becomes

$$E_k{}^{ex}=E^{MF}+K_1\cos k_z c+K_3(\cos k_x a+\cos k_y a), \quad (15)$$

where $K_1$ and $K_3$ represent the first- and third-nearest-neighbor coupling, respectively.

### C. Electric Dipole Processes in Magnetic Crystals

In considering the total electric dipole dispersion in a crystal such as $MnF_2$ where magnetic interactions are important, one must consider, in addition to the normal vibronic intensity source, the possibility of important magnon contributions. This means that the electronic excitation may couple either to an odd-parity phonon or magnon. In many nonmagnetic crystals, the phonon mechanism has been found to be very important. In $MnF_2$, magnon-assisted transitions have been clearly identified, but their total contribution to the electric dipole intensity has not yet been investigated. That they can be very important has been suggested by Lohr and McClure.[25] They have found that for many $Mn^{+2}$ salts, the temperature dependence expected for phonon-assisted electric dipole transitions does not occur, and that the intensity variation among these salts is a function of the coupling between the ions in the lattice.

TABLE I. Sideband selection rules.

| Exciton | Magnetic dipole selection rules | 2nd-neighbor coupling | 1st-neighbor coupling | 3rd-neighbor coupling |
|---|---|---|---|---|
| $\Gamma_1^+$, $\Gamma_2^+$ | $\sigma$ | $\pi(50.4)^a\sigma(54.8)$ | $\sigma(-)^b$ | $\pi(-)$ |
| $\Gamma_3^+$, $\Gamma_4^+$ | $\pi$ | $\pi(54.8)$ $\sigma(50.4)$ | $\pi(-)$ | $\sigma(-)$ |

[a] Numbers in parentheses are the energies of the effective critical points in the magnon density of states for terms containing $u_k$.
[b] Dashes in parentheses indicate that the critical points in the magnon density of states are not effective in producing intensity.

The following is a list of processes which might provide a significant source of intensity in the parity- and spin-forbidden transitions in magnetic crystals: (a) the relatively small contribution ($f<10^{-9}$) of no-phonon, no-magnon magnetic dipole transitions, (b) no-phonon, magnon-assisted electric dipole sidebands such as have been identified, (c) no-phonon, multi-magnon sidebands, (d) magnon-assisted sidebands with accompanying magnons, and (f) no-magnon, phonon-assisted transitions (normal vibronic transitions).

To ascertain the contribution of magnon-assisted transitions to the total intensity, it is helpful to consider the analogy between this process and that of a phonon-assisted transition. In a phonon-assisted transition, the total intensity is distributed according to the Franck-Condon principle. Such a distribution should occur as well in the case of magnon-assisted transitions, the spin-wave sidebands acting as the no-phonon origins. Thus the magnon-assisted process may contribute considerably more spectral intensity than appears in the no-phonon magnon sidebands.

We can set a lower limit to the total magnon-assisted contribution by noting that the magnetic dipole intensity is also distributed according to the Franck-Condon principle. In a previous paper[15] we have determined the fraction of the total magnetic dipole intensity for each cubic field state appearing in its magnetic dipole origins. We assume that this same fraction (called $f_{cal}/f_{obs}$ in Ref. 15) gives the ratio of the strength of the magnon origin to the total spectrum associated with it. We may not always be able to identify the no-phonon magnon sidebands corresponding to the higher sublevels of a cubic field state. Hence we can put only a lower limit on the total magnon-assisted contribution. The difference between the magnon-assisted contribution and the observed intensity then sets an upper limit on the vibronic contribution.

[25] L. L. Lohr and D. S. McClure, J. Chem. Phys. 49, 3516 (1968).

An external magnetic field can be useful in determining whether or not a magnon is involved in the relatively sharp features on the electric dipole envelopes. Since the electric dipole moment operator is spin-independent, eigenfunctions which describe the initial and final states of the transition must contain a component of the same spin projection. The two-sublattice ground state has a spin projection which is essentially zero. For the magnon, $M_s=\pm\frac{3}{2}$. Therefore the electronic excitation to which the magnon is coupled must contain a component $M_s=\mp\frac{3}{2}$. The sideband intensity is then proportional to the square of the coefficient of the component $M_s=\mp\frac{3}{2}$ in the wave function of the excited state. If the $g$ values of the ground and excited electronic states are nearly identical, as they are for $MnF_2$,[3] then we expect the major portion of the magnon-assisted intensity to be unaffected by the magnetic field. In general, however, a phonon absorption will behave in the same way as its electronic origin, and should split in a magnetic field.

Magnon sidebands of excited states for which $M_s$ is not exactly $\mp\frac{3}{2}$ will be split in a magnetic field by an amount dependent upon the deviation from $M_s=\mp\frac{3}{2}$. The magnetic behavior of sidebands involving more than one magnon should obey the same rules as apply to the single-magnon process if the transition is also induced by the spin-independent electric dipole moment operator. Examples of most of the foregoing types of absorption bands will be discussed in the following sections of this paper.

## III. EXPERIMENTAL TECHNIQUES

For most of this work, we used crystals obtained from Stout.[26] The impurity concentration of these crystals was about 100 ppm. However, we also obtained two crystals from Guggenheim with impurity concentrations of less than 20 ppm. This enabled us to identify any impurity lines. The crystals were oriented either by means of a polarizing microscope or by x rays.

Intensity measurements were made photoelectrically, using a 3.4-m Jarrell Ash spectrograph with a 30 000-lines/in. grating in the first order, giving a dispersion of 2.5 Å/mm. The light source was supplied by a stabilized power supply in order to minimize noise in the signal, which was 0.4% for most of this work. Thus we could measure optical densities as small as 0.002 units.

Most of the studies in high magnetic fields were made utilizing a pulsed magnet, described previously.[27] In most of these experiments, the magnetic field was along either the $c$ axis or 45° to the $a$ axis. However, we have also performed some experiments with components of the magnetic field along both the $c$ axis and the basal plane. These were performed by tilting the crystal so that the $c$ axis made an angle of about 15° to the magnetic field and so that the projection of the magnetic field was in the desired direction in the basal plane. Unfortunately, with the crystal in this configuration the magnetic transition appears to occur gradually,[28,29] so that with **H**, at an angle of 15° to the $c$ axis, even a 170-kG field does not completely reorient the spins. Such experiments will only indicate the direction of spectral changes as the flopped field condition is approached.

The apparatus used to perform uniaxial strain experiments consisted of two concentric stainless-steel tubes. The crystal was sandwiched between the sealed ends of these tubes. Between the inner tube and the sample was placed a ball bearing and short rod, the surface of which applied pressure to the crystal through a 3-mil Mylar film. The stress was determined from the air pressure over the piston which applied the stress. Although the stress experiments were done mainly to aid us to associate zero magnon origins with magnon sidebands, we have attempted to obtain reliable stress coefficients. This required careful attention to crystal shape, size, polish, and careful force measurements.

The Dewar which was used for all experiments, exclusive of those in a magnetic field, was arranged so that the temperature could be varied by adjusting the pressure of helium exchange gas surrounding the sample and by applying current to a heating element. Alternatively, at low temperatures, helium could be condensed in the sample compartment. Temperatures were determined either from the resistance of an Allen-Bradley 68-Ω carbon resistor or from the potential across a copper-constantin thermocouple. These were most useful below and above 20°K, respectively. These temperature sensors were in thermal contact with the copper block on which the sample was mounted. In the temperature range 15–30°K, the region in which the hot bands were investigated, the temperature accuracy was approximately ±1°K.

## IV. OBSERVATIONS OF SIDEBANDS AND THEIR INTERPRETATION

We have previously reported some preliminary results on the absorption to several of the excited states of the $Mn^{2+}$ ion in $MnF_2$.[27] We now present these observations in detail, and attempt an interpretation of the properties of the absorption bands.

For most of the excites states examined, the absorption has the following pattern. At helium temperatures, the origin of the absorption consists of a sharp, purely polarized, magnetic dipole line which splits in an external magnetic field applied along the $c$ axis. About 50 $cm^{-1}$ to the blue of the origin, a much more intense electric dipole absorption occurs which is unaffected by an external magnetic field applied along the $c$ axis. An

[26] M. Griffel and J. W. Stout, J. Am. Chem. Soc. **72**, 4351 (1950).
[27] D. S. McClure, R. Meltzer, S. A. Reed, P. Russell, and J. W. Stout, in *Optical Properties of Ions in Crystals*, edited by H. M. Crosswhite and H. W. Moos (Wiley-Interscience, Inc., New York, 1967), p. 257.
[28] I. S. Jacobs, J. Appl. Phys. **32**, 615 (1961).
[29] H. Rohrer and H. Thomas (to be published).

TABLE II. Properties of absorption lines below the flop-field transition.

| State | Line and polariaztion | $T$(°K) | Energy ($cm^{-1}$) | Full width at half-height ($cm^{-1}$) | $\frac{\Delta E}{2\beta H}$ [a] | [001] strain shift for $10^3$ kg/cm$^2$ ($cm^{-1}$) | Analysis ($cm^{-1}$) | $10^{11} f_{obs}$ [b] |
|---|---|---|---|---|---|---|---|---|
| $^4T_1$(I) | $H1\sigma$ | 25 | 18 369.1±0.5 | 16 | | −21.0 | −49.3 | 7.2 |
| | $M1\sigma$ | 4.2 | 18 418.4±0.1 | 0.75 | 1.79 | −20.3 | | 5.25±0.3 |
| | $M2\sigma$ | 4.2 | 18 435.3±0.1 | 1.1 | 1.90 | −2.0 | | 4.5 ±0.3 |
| | $E1\pi$ | 4.2 | 18 459.9±0.4 | 13 | 0.0 | −19.0 | 41.5 | 150 ±10 |
| | $E1\sigma$ | 4.2 | 19 475.4±0.2 | 3.4 | 0.0 | −19.5 | 57.0 | 100 ±10 |
| | $E2\sigma$ | 4.2 | 18 483.6±0.3 | 5.0 | 0.0 | −2.6 | 48.3 | 140 ±10 |
| | Total $\sigma$ | 4.2 | | | | | | 20 000 |
| | Total $\pi$ | 4.2 | | | | | | 18 700 |
| $^4T_2$(I) | | 4.2 | Broad band with no sharp features | | | | | |
| $^4A_1$, $^4E$(I) | $H4\sigma$ | 33 | 25 056 ±10 | | | | | |
| | $H3\sigma$ | 33 | 25 097 ±10 | | | | | |
| | $H2\sigma$ | 33 | 25 139 ± 5 | ∼50 | | | | |
| | $H2\pi$ | 33 | 25 153 ± 5 | ∼50 | | | −107 | |
| | $H1\sigma$ | 20 | 25 194.6±0.6 | 10 | 0.0 | 2.8 | −51.0 | |
| | $E2\pi a$ | 4.2 | 25 239.1±0.3 | 0.7 | 0.0 | 0.6 | −21.0 | |
| | $E2\pi$ | 4.2 | 25 240.7±0.3 | 3.2 | 0.0 | 0.6 | −19.4 | 2 600±300 |
| | $M1\sigma$ | 4.2 | 25 245.6±0.1 | 1.7 | 1.96 | 2.8 | 0 | 50±8 |
| | $M2\pi$ | 4.2 | 25 260.1±0.1 | 1.5 | 2.04 | 1.0 | 0 | 91±18 |
| | $E1\pi$ | 4.2 | 25 293.2±0.4 | 6.5 | 0.0 | 2.7 | 47.6 | 435 ±60 |
| | $E1\sigma$ | 4.2 | 25 295.1±0.5 | 20 | 0.0 | 2.9 | 49.6 | ∼3 000 |
| | $E2\sigma$ | 4.2 | 25 311 (edge) | | 0.0 | 1.3 | | 9 000 |
| | $E3\pi$ | 4.2 | 25 343 ±2 | 6 | 2.0 | | | |
| | $E4\pi$ | 4.2 | 25 388 ±2 | 10 | 0.0 | | | |
| | $E5\pi$ | 4.2 | 25 403 ±2 | 10 | 2 | | | |
| | $E6\sigma$ | 4.2 | 25 438.1±0.6 | 25 | 0.0 | | | ∼ 900 |
| | $E6\pi$ | 4.2 | 25 443.9±0.5 | 25 | 0.0 | | | ∼11 000 |
| | $E7\pi$ | 4.2 | 25 492 ±5 | 15 | 2 | | | |
| | Total $\sigma$ | 4.2 | | | | | | ∼24 000 |
| | Total $\pi$ | 4.2 | | | | | | ∼19 500 |
| $^4T_2$(II) | $H1\pi$ | 20.0 | 27 928.1±0.8 | 18 | 0 | <1.5 | −55.0 | 22.5 |
| | $H1\sigma$ | 25 | 27 946.5±3 | 30 | | | −36.6 | |
| | $M1\pi$ | 4.2 | 27 983.1±0.4 | 1.3 | 1.76 | <0.5 | | 0.75±0.1 |
| | $E1\pi$ | 4.2 | 28 024.6±0.6 | 3.5 | 0.0 | <1.0 | 41.5 | 1 100 |
| | $E1\sigma$ | 4.2 | 28 026.8±0.4 | 9 | 0.0 | <1.0 | 43.7 | 1 700 |
| | $E2\sigma$ | 4.2 | 28 163.5±3 | 15 | 0.0 | | | |
| | $E4\sigma$ | 4.2 | 28 241 ±2 | 18 | 0.0 | | | |
| | $E4\pi$ | 4.2 | 28 242.0±2 | 15 | 0.0 | | | |
| | $E6\pi$ | 4.2 | 28 345.2±2 | 10 | 1.8 | | | |
| | $E7\sigma$ | 4.2 | 28 373.9±3 | 15 | 0 | | | |
| | $E8\sigma$ | 4.2 | 28 427 ±5 | 25 | 0 | | | |
| | $E8\pi$ | 4.2 | 28 427 ±5 | 35 | 0 | | | |
| | $E9\sigma$ | 4.2 | 28 489 ±5 | 45 | 0 | | | |
| | $E9\pi$ | 4.2 | 28 489 ±5 | 35 | 0 | | | |
| | Total $\sigma$ | 4.2 | | | | | | ∼15 000 |
| | Total $\pi$ | 4.2 | | | | | | ∼ 7 500 |
| $^4E$(II) | $H1\sigma$ | 25 | 29 848 | 20 | | | −45 | |
| | $H1\pi$ | 4.2 | 29 939.2±1 | 20 | 0.0 | | 46 | |
| | $E1\sigma$ | 4.2 | 29 943.5±1 | 20 | 0.0 | | 50 | |
| | $E2\sigma$ | 4.2 | 29 969 ±2 | 20 | | | | |
| | $E2\pi$ | 4.2 | 29 975.6±1 | 20 | 0.0 | | | |
| | Total $\sigma$ | 4.2 | | | | | | ∼ 1 900 |
| | Total $\pi$ | 4.2 | | | | | | ∼40 000 |
| $^4T_1$(II) | $M1\pi$ | 4.2 | 31 940.6±0.3 | 4.4 | 2.0 | +5.7 | | 83±7 |
| | $E2\sigma$ | 4.2 | 32 067.4±0.5 | 12 | 1.8 | 7.0 | | 100±22 |
| | $E2\pi$ | 4.2 | 32 067.1±0.5 | 15 | 1.8 | 5.9 | | 165±30 |
| | Total $\sigma$ | 4.2 | | | | | | ∼37 000 |
| | Total $\pi$ | 4.2 | | | | | | ∼25 000 |

[a] Errors are ±0.1. Data obtained by remeasurement of plates of P. G. Russell (Ref. 34).
[b] $f = 6.48 \times 10^{-9} \int \epsilon(\bar{\nu}) d\bar{\nu}$. For the $H \perp c$ ($\pi$) magnetic dipole transitions, $\epsilon$ was obtained by taking the $Mn^{+2}$ concentration to be half the ions in the crystal. Most of these data were obtained by our integration of the absorption curves of J. W. Stout and S. A. Reed (Ref. 16).

examination of the electric dipole absorption indicates that it is highly polarized. Further to the blue, the absorption appears to be almost completely electric dipole and considerably broader. The features of this absorption indicate that it is also highly polarized. Some of these features split in a magnetic field like the magnetic dipole origin, while others behave like the sidebands. As the temperature is raised above 15°K,

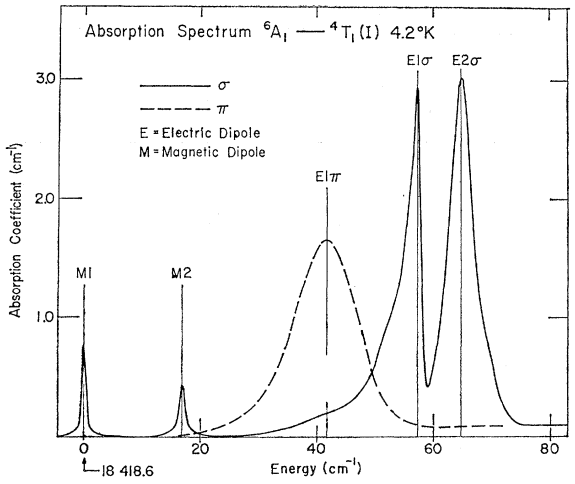


FIG. 2. Absorption near the origin of the transition $^6A_1 \rightarrow {}^4T_1$(I) at 4.2°K.

electric dipole absorption appears about 50 cm$^{-1}$ to the red of the origin. Its temperature dependence indicates that this absorption arises from the thermal population of a state about 50 cm$^{-1}$ above the ground state. This hot-band absorption is unaffected by an external magnetic field.

In Table II the properties of the absorption to six of the cubic field states of $MnF_2$ are summarized.[30] The effects of an external magnetic field and a uniaxial stress along the $c$ axis are presented. The absorption lines are identified in this table by three symbols.[31] The first, consisting of the letters $M$, $E$, or $H$, indicates magnetic dipole, electric dipole cold-band and electric dipole hot-band absorption, respectively. The second, an arabic number, distinguishes the prominent absorptions of a particular type in order of increasing energy. The numbering looks ahead to the associations between the origins and their sidebands which we shall find in the following discussion. The last symbol indicates the polarization of the absorption. The $\pi$ and $\sigma$ polarizations correspond to absorption polarized with the electric vector parallel and perpendicular to the $c$ axis, respectively.

The experimentally determined oscillator strengths in Table II were obtained from the expression[32]

$$f=\frac{mc^2}{\pi e^2}\left(\frac{E_0}{E_{\text{eff}}}\right)^2\frac{n}{N}\int\alpha(\bar{\nu})d\bar{\nu}=6.57\times10^{-11}\int\alpha(\bar{\nu})d\bar{\nu}, \quad (16)$$

if we take for the refractive index $n=1.5$ and for the effective field correction $E_0/E_{\text{eff}}=1$. In this expression, $\alpha(\bar{\nu})$ is the absorption coefficient in units of cm$^{-1}$ and $N$ is the number of ions per cm$^3$. If we assume a unidirectional transition moment for the single-ion magnetic dipole transitions under the $C_{2h}$ site symmetry, we must take, for $\mathbf{H}\perp c$ ($\pi$) transitions, only half the total number of $Mn^{+2}$ ions, since sites on the two sublattices are mutually orthogonal.

For cases where the associations between the origins and the sidebands appear to be well established, we attempt to derive values for the exciton dispersion parameters by fitting calculated line shapes for various values of the exciton dispersion to the observed sidebands. The line shapes were calculated by a Monte Carlo integration of Eq. (7). For the hot bands, the renormalization factor was found by an iterative solution of Eqs. (12) and (13). A major difficulty in making such an analysis for the cold bands is the possibility of exciton-magnon interactions. This problem can be avoided by first analyzing the hot-band absorption (or temperature-independent emission) line shapes, since in these transitions the exciton and magnon do not coexist. The resulting exciton dispersion parameters can then be applied to the cold bands to determine the exciton-magnon interaction. Such an approach, however, still suffers from several difficulties, which include the assumptions made about the range of the coupling mechanism producing the absorption and the form of the exciton dispersion, as well as the possibility of magnon-phonon interactions, which might be important at the temperatures required to observe the hot bands. A further difficulty arises from the presence of two independent parameters in the expression for the absorption in one polarization due to second-nearest-neighbor coupling. With zero exciton dispersion, the two terms will give contributions to the total line shape which peak at the same energy but which have different linewidths, the $\pi_A$ term giving a much narrower line than the $\pi_Z$. For $K_1\neq0$, $K_3=0$, the peaks will be shifted by the same amount. However, for nonzero values of $K_3$, the peak arising from the $\pi_A$ term will be shifted to a greater extent and as a result the over-all peak position will depend on the relative contributions of the $\pi_A$ and $\pi_Z$ terms.

### A. $^4T_1$(I) State: 18 500 cm$^{-1}$

A rigorous examination of the cold-band magnon absorption to this state has been undertaken by Sell *et al.*[2] They observe two magnetic dipole lines, $M1\sigma$ and $M2\sigma$, followed by three electric dipole absorptions, $E1\pi$, $E1\sigma$, and $E2\sigma$ shown in Fig. 2. Sell *et al.*[2] and Russell *et al.*[3] identified these electric dipole absorptions as magnon sidebands, based upon their line shapes, temperature dependence, and behavior in an external magnetic field. Dietz *et al.*,[4] by examining these transitions in a uniaxial stress along the [001] and [110] directions, have determined that $M1\sigma$ is an origin for

[30] Note that with regard to transitions to the $^4T_1$(I) state, the half-widths of the magnetic dipole transitions and all the oscillator strengths reported here differ from the values given in Ref. 2. This results from both a different choice for the oscillator-strength expression and apparently a real difference in the measured integrated absorption.

[31] This notation differs from that used in Refs. 1 and 2, where $M$ represented magnon sideband, and in Ref. 4, where $E$ described the pure electronic transition to an exciton state.

[32] D. L. Dexter, *Solid State Physics* (Academic Press Inc., New York, 1958), Vol. 6, p. 353.

$E1\pi$ and $E1\sigma$, whereas $M2\sigma$ is the origin of $E2\sigma$. This conclusion is based on the assumption that the magnon dispersion is unaffected by the strain. Hence lines which respond in the same way to strain arise from the same electronic sublevel.

Sell *et al.*, have been able to fit the line shape of $E1\sigma$ quite well, using the known magnon dispersion and a positive exciton dispersion of $K_1=-1.3$ cm$^{-1}$, $K_3=0$. They find, however, that $E1\pi$ must be described with the different parameters $K_1=-1.3$ cm$^{-1}$, $K_3=4.3$ cm$^{-1}$. Such a relatively large third-nearest-neighbor coupling appears unreasonable, as pointed out by the above authors and fails any longer to describe $E1\sigma$. The line shape for $E2\sigma$ has been described previously[2] by the parameters $K_1=3.1$ cm$^{-1}$, $K_3=0$.[2] However, the higher-energy side of the line is fitted better by using the parameters $K_1=3.5$ cm$^{-1}$, $K_3=-2.0$ cm$^{-1}$. Since only one sideband of any kind is observed for this state, there is no other indication of the validity of these values.

Misetich *et al.*,[5] have observed, in carefully purified crystals, intrinsic emission corresponding to $M1\sigma$. They observe the emission to the ground state and to a single-magnon state, both in the $\sigma$ polarization. They find that the sideband line shape can be fitted quite well by considering only first-neighbor intrasublattice coupling. This conclusion is based upon the failure to observe any $\pi$-polarized emission and on the ratio of intensity of the sideband to that of the origin, which is forty times greater than that which calculations based on intersublattice coupling predict. Noting the temperature independence of the intensity and line shape of the emission sideband between 1.3 and 2.5°K, they can set an upper limit of 1 cm$^{-1}$ on the exciton dispersion of $M1\sigma$. Based on a study of the effect of [100] stress, in which it was found that while the shape and position of $E1\sigma$ and $E2\sigma$ were drastically affected by an anticrossing of the two excitons, the intrinsic emission was not, Dietz and Misetich[33] confirmed that $M1\sigma$ has no measurable dispersion, and determined that neither did $M2\sigma$. The difficulties in calculating the line shapes of the sidebands $E1\sigma$, $E2\sigma$, and $E1\pi$ must therefore arise from some cause other than the excition dispersion—probably a strong exciton-magnon or exciton-phonon interaction.[2]

We have studied the very weak temperature-dependent $\sigma$-polarized absorption in this state as reported earlier.[27] It can be seen from Table II that this hot band, $H1\sigma$, has the same energy behavior as $M1\sigma$ as a function of stress, indicating that $M1\sigma$ is its origin. No $\pi$-polarized hot-band absorption is observed.

If the absorption strength of $H1\sigma$ is corrected for the population of the magnons in the ground state, using Bose statistics, it is found that the ratio of the intensity of $H1\sigma$ to that of $M1\sigma$ is 10, in fair agreement with the value of 6 found for the intrinsic emission.[5]

[33] R. E. Dietz and A. Misetich, *Localized Excitations in Solids* (Plenum Press, Inc., New York, 1968), p. 366.

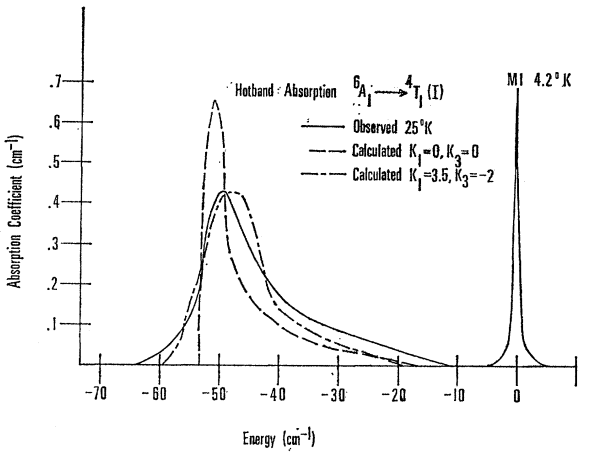


FIG. 3. Observed and calculated line profiles of $H1\sigma$ of the transition $^6A_1 \rightarrow {}^4T_1$(I) at 25°K. The solid curve represents the observed absorption, while the broken curves give the calculated line shapes (see text). The area under the calculated curves has been chosen to be equal to that under the observed one.

We suggest, therefore, that $H1\sigma$ arises from the same first-nearest-neighbor coupling responsible for the intrinsic emission. In Fig. 3 the observed line shape at 25°K is compared to that calculated by assuming first-nearest-neighbor interaction at this temperature with no exciton dispersion. The peak agrees reasonably well with the observed one, but the calculated hot-band appears much too narrow. The observed breadth may indicate the presence of important magnon-phonon interactions. It should be noted that if the breadth of the line is not used as a criterion of the fit of the calculated hot band, then there are many sets of values for the exciton dispersion parameters which will give the correct peak position. If $K_1$ is taken to be some positive (negative) value, then, in general, a negative (positive) value of $K_3$ can be found which will give the desired peak position. One such set of parameters, which gives approximately the correct linewidth, is also shown in Fig. 3.

We find no clear evidence for a hot band to $M2\sigma$. Such a hot band is expected, since the intrinsic emission is still observed under sufficient [100] stress to produce an anticrossing between the two excitons.

### B. $^4T_2$(II) State: 28 000 cm$^{-1}$

The absorption of the $^4T_2$(II) state is shown in Figs. 4 and 5. Figure 4 indicates the complete absorption to this state at several temperatures. Figure 5 shows only the region about the magnetic dipole origin $M1\pi$. The prominent lines are labeled in these diagrams and their properties are listed in Table II. In an external magnetic field below the flop field, $M1\pi$ is split ($\Delta E/2\beta H=1.76$), whereas with the exception of line $E6\pi$, none of the electric dipole absorption appears to be affected by the field. This is demonstrated for the $\pi$ polarization in

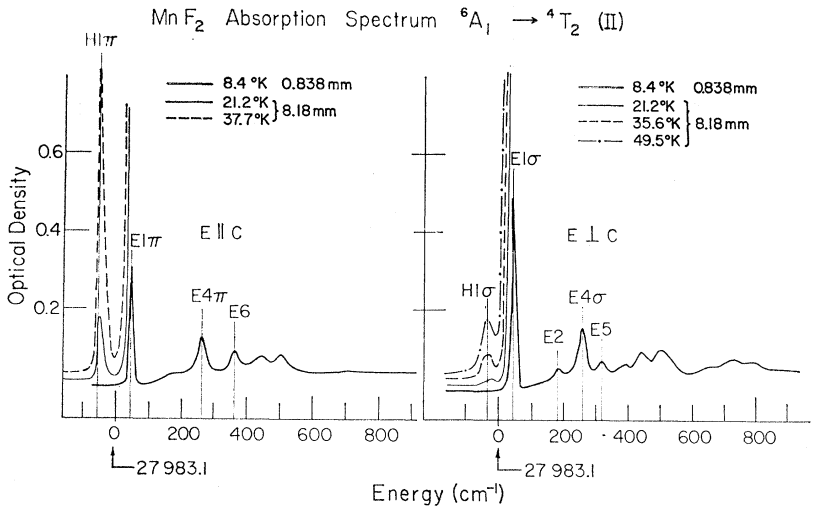


FIG. 4. Absorption of the transition $^6A_1 \rightarrow {}^4T_1$(II) at several temperatures. On the left and right are the absorptions of the $\pi$ and $\sigma$ polarizations, respectively. The absorption shown here is electric dipole. The zero of the abscissa indicates the energy of the magnetic dipole origin, too weak to be observed in these spectra. Note the different crystal thicknesses. These data were obtained from S. A. Reed, and J. W. Stout (unpublished results).

Fig. 6.[34] Above the flop field, the hot band $H1\pi$ shifts by $+45$ cm$^{-1}$, as do the temperature-independent lines $E1\pi$ and $E1\sigma$.

The two unlabeled lines in Fig. 5 at 5 and 15 cm$^{-1}$ appear only in the least-pure samples. They are unaffected by magnetic fields up to 40 kG. We think, therefore, that they are magnon sidebands of electronic absorption occurring at $Mn^{+2}$ sites which are perturbed by neighboring impurities. These lines are then analogous to some of the sidebands observed in emission from the $^4T_1$(I) state, where the electronic excitation is trapped at $Mn^{+2}$ ions perturbed by impurities.

The insensitivity of $E1\pi$ and $E1\sigma$ to an external magnetic field and their energy separation from $M1\pi$ suggest that they are magnon sidebands of $M1\pi$ which arise, as do the sidebands of the $^4T_1$(I) state, predominantly from intersublattice second-nearest-neighbor coupling. The excited state of the transition $M1\pi$ is a $\Gamma_3^+$, $\Gamma_4^+$ exciton. From Table II we note that in the absence of exciton dispersion and exciton-magnon interaction we expect to see $E1\pi$ at 54.0 cm$^{-1}$ and $E1\sigma$ at 50.4 cm$^{-1}$ with respect to $M1\pi$. In fact, $E1\pi$ peaks at 41.5 cm$^{-1}$, which suggests a 13.3-cm$^{-1}$ negative-energy dispersion, i.e., $K_1 = 6.65$ cm$^{-1}$.

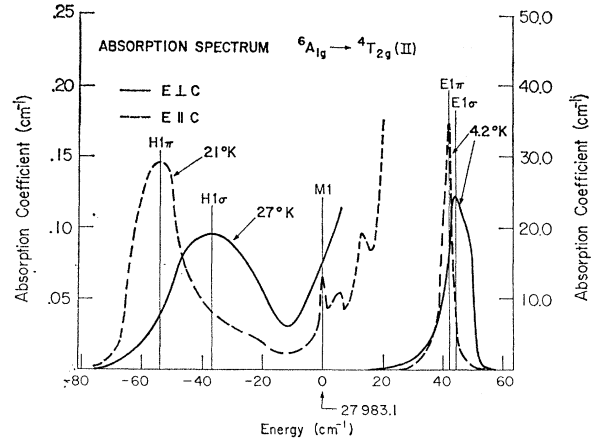


FIG. 5. Absorption near the origin of the transition $^6A_1 \rightarrow {}^4T_2$(II) at several temperatures. The ordinate on the right applies to the 4.2°K absorption curves, the ordinate on the left to the curves obtained at 21 and 27°K. The absorption at 5 and 15 cm$^{-1}$ results from $Mn^{+2}$ ions perturbed by impurity sites.

The calculated sidebands, assuming $K_1 = 6.65$, $K_3 = 0$, are given in Fig. 7. The peak position of the $\pi$ sideband will not depend on the relative values of $\pi_A$ and $\pi_Z$, since we have taken $K_3 = 0$. The calculated peak of $E1\pi$ agrees rather well. However, the calculated line is much too narrow, even when, as shown, the line is assumed to arise entirely from the $\pi_Z$ term. More important, this exciton dispersion does not give the correct shape for $E1\sigma$. The calculated line peaks at 50.4 cm$^{-1}$, while the observed line peaks at 44 cm$^{-1}$ and has a shoulder at about 50 cm$^{-1}$. A series of calculations was made in which $K_1$ and $K_3$ were varied so as to leave the peak of $E1\pi$ at about 41 or 42 cm$^{-1}$, but nothing resembling the observed shape of $E1\sigma$ could be obtained.[35] Again it is possible that either longer-range coupling or exciton-magnon interactions may be important.

The hot band $H1\pi$ is relatively sharp and intense and stands out prominently at 25°K. Calculations based on the use of second-neighbor coupling as the source of intensity encountered the following difficulties: The computed intensity is from 5 to 130 times too weak, depending upon the proportion of $\pi_Z$ or $\pi_A$ which is assumed to predominate; the computed peak occurs at $-35^{-1}$, assuming no exciton dispersion, and is nearly the same with $K_1 = -6.65$ cm$^{-1}$, far from the observed value of $-55$ cm$^{-1}$. Since first-neighbor coupling is expected to contribute to the sideband intensity of a $\Gamma_3^+$, $\Gamma_4^+$ exciton, this is undoubtedly the major source of intensity of $H1\pi$. In fact, the calculated line shape and

[34] P. G. Russell and D. S. McClure (unpublished results).

[35] The situation bears some resemblance to that in the $^4T_1$(I) state where again a single set of parameters will not reproduce the observed shapes of both $\sigma$ and $\pi$ absorption.

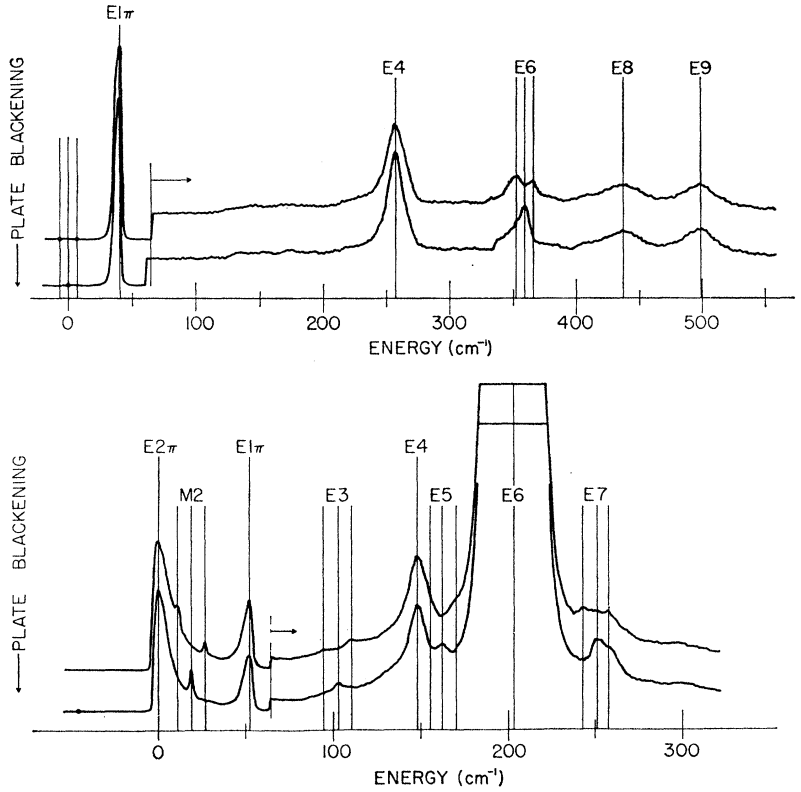


FIG. 6. Effect of 80-kG magnetic field along the $c$ axis on the $\pi$-polarized absorption to the $^4T_2$(II) and the $^4A_1$, $^4E$(I) states. Absorption to the $^4T_2$(II) state is shown in the upper pair of traces, absorption to the $^4A_1$, $^4E$(I) in the lower. The upper and lower traces of each pair were made with magnetic fields of 80 and 0 kG, respectively. To the right of the arrows, the recorder sensitivity was increased. The triplet of vertical lines serves to indicate the splitting of the transitions in a magnetic field. The splitting of the origin of the $^4T_2$(II) absorption is indicated by the dots on the left [from plates of Russell (Ref. 34)].

peak position at 21°K, with $K_1=6.65$ cm$^{-1}$, agree completely with the observations made on $H1\pi$. These properties are rather insensitive to the exciton dispersion, but a series of calculations for several sets of values suggests strongly that $K_1>4$, $K_3<1.5$ cm$^{-1}$. This together with the evidence just presented for the cold-bands confirms that there is appreciable negative exciton dispersion arising chiefly from exchange with first neighbors in the $^4T_2$(II) state.

$H1\sigma$ must result either from third-neighbor intra-sublattice or second-neighbor intersublattice coupling. Both processes quench any intensity at the zone edge, since at the zone edge, $\sin^2 k_x a=\sin^2 k_y a=0$ and $v_k^2=0$. Both processes involve $\Delta M_S=0$ transitions and are therefore not split by an external magnetic field. The line shapes found for the two different couplings are also given in Fig. 7 for the exciton dispersion $K_1=6.65$, $K_3=0$. The intersublattice coupling gives a very good fit to the shape, although the observed peak is 5 cm$^{-1}$ further to the red, while the third-neighbor shape is quite unsatisfactory. We may also compare the observed intensity ratio of $H1\sigma$ and $E1\sigma$ with the calculated ratio obtained using the second-nearest-neighbor hot band, since the parameters for the intersublattice coupling mechanism are the same in both cases. We find that the observed intensity ratio is about 90 at 27°K, while the calculated ratio at this temperature is about 120, indicating that the coupling to the opposite sublattice is indeed giving rise to the transition. The very broad $H1\sigma$ absorption is very insensitive to changes of a few wave numbers in exciton dispersion and thus gives no more information about it.

The behavior of the $\pi$-polarized absorption of the $^4T_2$(II) state in an 80-kG magnetic field is shown in Fig.

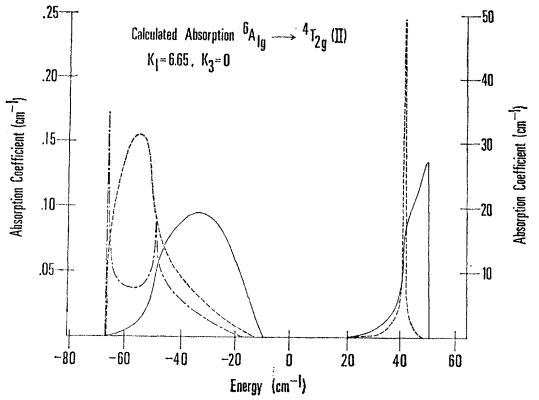


FIG. 7. Calculated line profiles for the transition $^6A_1 \rightarrow {}^4T_2$(II) using the parameter $K_1=6.65$, $K_3=0$. Cold-band absorption arising from second-neighbor coupling (to the right of the origin): solid curve, $\sigma$; short-dashed curve, $\pi(\pi_Z\neq 0, \pi_A=0)$. Hot-band absorption (to the left of the origin): solid curve, $\sigma$, second-neighbor coupling, 20°K; long-dash–short-dash curve, $\sigma$, third-neighbor coupling, 25°K; short-dashed curve, $\pi$, first-neighbor coupling, 25°K. The area under the curves has been taken to be equal to that of the corresponding experimental curves, except for the $\pi$ cold band, which is too narrow, and the third-neighbor coupling $\sigma$ hot band, whose area is represented as one-half that of the observed $\sigma$ hot band.

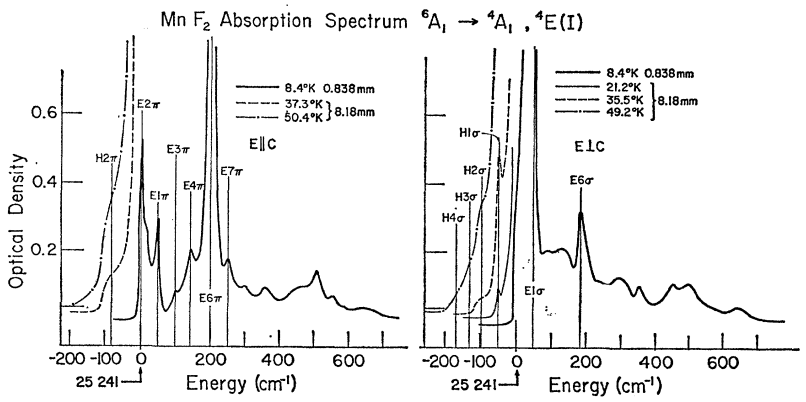


FIG. 8. Absorption of the transition ${}^6A_1 \rightarrow {}^4A_1$, ${}^4E(\mathrm{I})$ at several temperatures. On the left and right are the absorptions in the $\pi$ and $\sigma$ polarizations, respectively. Only the electric dipole absorption is shown. Note the different crystal thicknesses. These data were obtained from S. A. Reed and J. W. Stout (unpublished results).

6. With the exception of $E6\pi$, the electric dipole absorption is unaffected by the field. This is true without exception in the $\sigma$ polarization. On the basis of the discussion of Sec. II C, it appears that most of this absorption must be magnon-assisted. $E6\pi$ may be interpreted either as a magnon sideband of an unobserved electronic sublevel of predominantly $M_s=\mp\frac{1}{2}$ character, but sufficient $M_s=\mp\frac{3}{2}$ character to provide the intensity, or as a phonon sideband of a $M_s=\mp\frac{3}{2}$ electronic sublevel.

### C. ${}^4A_1$, ${}^4E(\mathrm{I})$ States: 25 000 cm$^{-1}$

In many respects the absorption to this state is the most interesting in the spectrum. The whole absorption band at several temperatures is shown in Fig. 8. In Fig. 9 the region near the origin is shown at 4.2°K. The properties of the prominent absorption bands are listed in Table II. The interesting properties of transitions to this state are (a) the sharp cutoff of the absorption at the low-energy side of the spectrum, (b) the very sharp electric dipole spike at the origin, (c) the occurrence of a progression of at least four hot bands, and (d) the intensity of the electric dipole absorption about the origin which is an order of magnitude stronger than that of any other state.

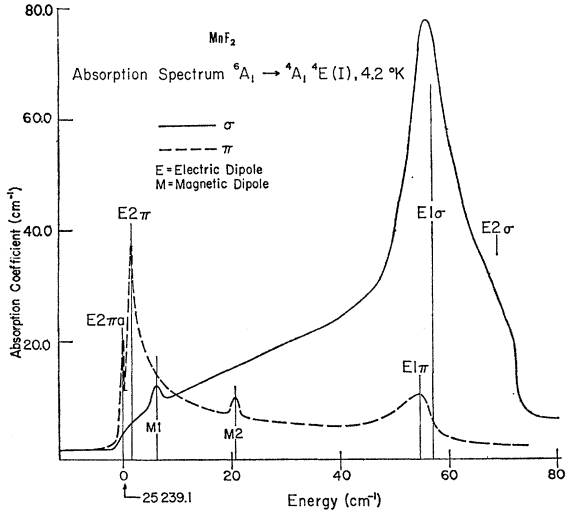


FIG. 9. Absorption near the origin of the transition ${}^6A_1 \rightarrow {}^4A_1$, ${}^4E(\mathrm{I})$ at 4.2°K.

Spin-orbit coupling does not split these cubic field states to first order. $M_s$ is then a good quantum number. We therefore expect to see three single-ion magnetic dipole transitions and their associated magnon sidebands corresponding to the three $M_s=\mp\frac{3}{2}$ orbital components of ${}^4A_1$, ${}^4E(\mathrm{I})$. It can be seen from Fig. 9 that two of these, $M1\sigma$ and $M2\pi$, are observed.[15] They have the expected intensity and magnetic field splittings, and correspond to $\Gamma_1^+$, $\Gamma_2^+$ and $\Gamma_3^+$, $\Gamma_4^+$ excitons, respectively. These two transitions are probably to the two orbital components of ${}^4E(\mathrm{I})$.

The electric dipole absorptions about $M1\sigma$ and $M2\pi$ are unaffected by an external magnetic field of magnitude less than the flop field. They presumably arise from a superposition of sidebands to $M1\sigma$ and $M2\pi$. The very strong electric dipole absorption $E6\pi$ is probably a sideband to the $M_s=\mp\frac{3}{2}$ ${}^4A_1$ state.[15] This implies that $E2\pi$ and $E2\pi a$ are sidebands which occur at lower energies than their origin. We have looked carefully for magnetic dipole transitions at lower energies, and have found none.

In order to try to associate the sidebands with $M1\sigma$ and $M2\pi$, we have applied an uniaxial stress along the [001] crystallographic axis. The observations are shown in Fig. 10. The transitions $M1\sigma$, $E1\pi$, and $H1\sigma$ all have nearly the same behavior under 001 stress, namely, they increase by $2.75\pm0.1$ cm$^{-1}$ for each $10^3$ kg/cm$^2$ of applied stress, as shown in Fig. 10, and we now conclude that they all belong to one electronic origin, $M1\sigma$. The experiments were done several times with crystals of differing thickness. Crystals 0.33 mm thick had to be used to observe the behavior of the intense $E1\sigma$ line. In these latter experiments it became clear that the shoulder which we have called $E2\sigma$ has a different stress dependence from the peak $E1\sigma$ and must therefore belong to a different electronic origin. By observing the high-frequency edge of this band the stress behavior shown in Fig. 10 was obtained, amounting to about 1.3 cm$^{-1}$ per $10^3$ kg/cm$^2$ of applied 001 stress. This is close

enough to the value 1.0 found for $M2\pi$ to be interpreted as a sideband of $M2\pi$. The lines $E2\pi$ and $E2\pi a$ shift by about 0.6 $cm^{-1}$. Although this is appreciably less than the shift in $M2\pi$, we associate these lines with $M2\pi$ as origin, and will discuss the difference in their stress behavior shortly. The very strong band $E6\pi$ has almost no shift under stress. A slight narrowing and a slight change of shape were observed. This behavior reinforces our conclusion stated above, that $E6\pi$ is a sideband of an unobserved magnetic dipole origin, since neither $M1\sigma$ nor $M2\pi$ has such a stress dependence. The 001 stress experiments have thus been successful in permitting us to associate the two magnetic dipole origins with all of their single-magnon sidebands, and we may now consider the interpretation of the sidebands in detail. The positions, absorption strengths, and stress dependence of these bands are summarized in Table II.

Since the magnon sidebands $E2\pi$ and $E2\pi a$ are at lower energies than their origin, this exciton must have a very large negative-energy dispersion near the $Z$ point of the Brillouin zone. Such a dispersion could arise from a large excitation exchange between $Mn^{+2}$ ions along the $c$ axis. The absorption in the $\sigma$ polarization due to the magnon sideband begins at an identical energy to that of the $\pi$ polarization, since as one moves away from the $Z$ point, intensity can occur in both polarizations. However, the major part of the $\sigma$-polarized sideband absorption occurs at considerably higher energies, indicating that the excitation exchange in the basal plane is small.

The $M2\pi$ sideband absorption is reproduced by the dispersion $K_1=37$ $cm^{-1}$, $K_3=0$ ($K_3=2$ $cm^{-1}$ gives the shoulder position in the $\sigma$ spectrum more accurately but does not reproduce the low-energy cutoff of $E2\pi$), while small negative exciton parameters, $K_1=2$ $cm^{-1}$, $K_3=1$ $cm^{-1}$, best fit the cold-band absorption associated with $M1\sigma$. The superposition of cold bands resulting from $M1\sigma$ and $M2\sigma$ is shown in Fig. 11. While there are some differences between calculated and observed line shapes, the main features are fairly well reproduced by the calculations based upon the above parameters, particularly the line shapes of the sidebands to $M2\pi$. The sidebands to $M1\sigma$ appear too sharp in both polarizations. However, in this state, besides magnon-exciton interaction or longer-range effects, we might expect that interactions between the overlapping sideband levels could occur.

We can consider two sources for the intensity of $H1\sigma$, the prominent hot band associated with $M1\sigma$. The magnitude of $\pi_Z$ (due to second-neighbor coupling) derived from the cold band seems to be enough to explain $H1\sigma$, but because of the overlapping cold bands its value is not certain. The shape of $H1\sigma$ calculated on the assumption that its intensity is derived from second-neighbor coupling cannot be made to agree with the observed shape and peak position. A calculated band similar to that of $H1\sigma$ in Fig. 7 results, with a peak less

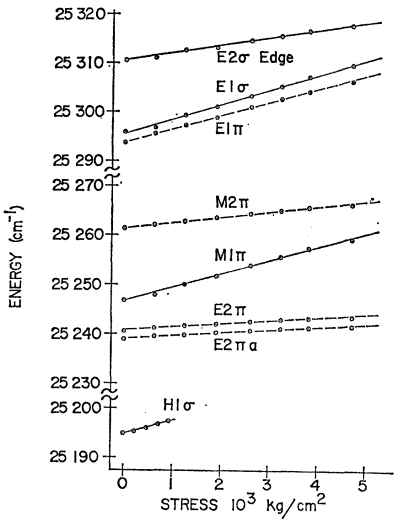


FIG. 10. Effect of [001] stress upon the absorption near the origin of the transition ${}^6A_1 \rightarrow {}^4A_1$, ${}^4E(I)$. Note the discontinuities in the ordinate.

than 40 $cm^{-1}$ below the exciton origin, even including the small negative exciton dispersion consistent with the cold bands of $M1\sigma$. On the other hand, the shape and position of $H1\sigma$ are consistent with first-nearest-neighbor coupling. The best fit is obtained using $K_1=0$, $K_3=0$, and is the same as for the ${}^4T_1(I)$ state, shown

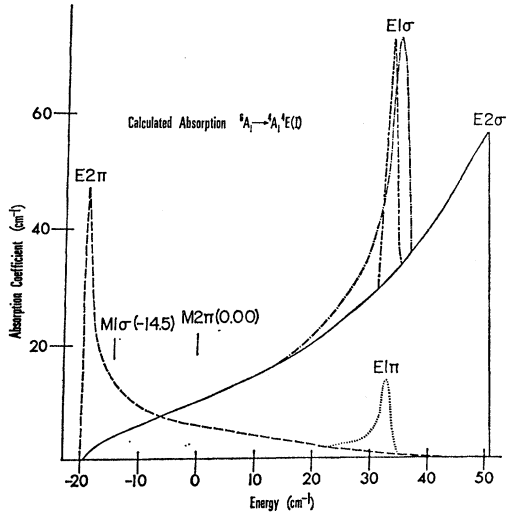


FIG. 11. Calculated cold-band absorption for the transition ${}^6A_1 \rightarrow {}^4A_1\,{}^4E$. Second-neighbor coupling only was included. Sidebands associated with the origin $M2\pi$: solid curve, $\sigma$; short-dashed curve, $\pi$, $\pi_Z \neq 0$, $\pi_A = 0$. These correspond to the parameters $K_1=37$ $cm^{-1}$, $K_3=0$ for the exciton dispersion. Sidebands associated with the origin $M1\sigma$ (shown superimposed on the $M2\pi$ absorption): dot-dashed curve, $\sigma$, $\pi_Z \neq 0$, $\pi_A = 0$; long-dash–short-dash curve, $\sigma$, $\pi_Z = 0$, $\pi_A \neq 0$; dotted curve, $\pi$. The exciton dispersion parameters $K_1=2$ $cm^{-1}$, $K_3=1$ $cm^{-1}$ were used. The areas under the calculated curves in the $\pi$ absorption were chosen to be equal to the observed area. Because of the superposition of absorption lines in the $\sigma$ polarization the absorption of individual lines is not known. Therefore for the $M2\pi$ absorption we have arbitrarily taken $\pi_X = 4\pi_Z$ and for the $M1\sigma$ absorption $\pi_Z = 4\pi_X$, $\pi_A = 2\pi_X$.

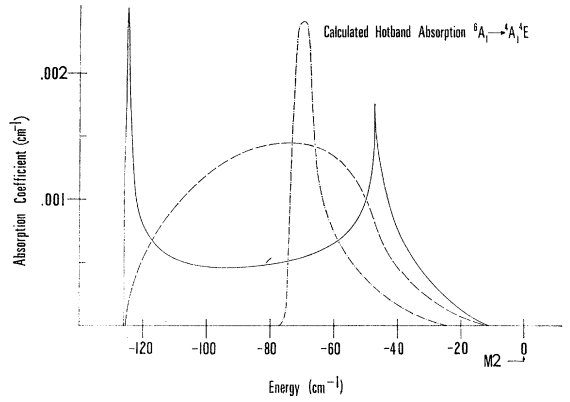


FIG. 12. Calculated hot-band absorption for the transitions $^6A_1 \rightarrow {}^4A_1\,{}^4E$. Absorption associated with $M2\pi$ ($K_1=37$, $K_3=0$); short-dashed curve, $\pi$, first-neighbor coupling, 36°K; solid curve, $\sigma$, third-neighbor coupling, 36°K. Absorption associated with $M1\sigma$ ($K_1=2$, $K_3=1$): dot-dashed curve, $\sigma$, first-neighbor coupling, 24°K. We have taken, for the $M_2\pi$ absorption, $\pi_1{}^\pi=1/C$, $\pi_3{}^\sigma=1/C$ and for the $M1$ absorption $\pi_1{}^\sigma=1/C$, where $C$ is the coefficient in Eq. (7).

in Fig. 3. The shape calculated using the exciton dispersion parameters derived for the cold bands is shown in Fig. 12. The small dispersion of $M1\sigma$ rules out the possibility that any of the other observed hot bands are associated with it, although the hot-band intensity due to second-nearest-neighbor coupling is presumably responsible for part of the steep background beneath $H1\sigma$.

Hot bands $H2\sigma$, $H3\sigma$, $H4\sigma$ and $H2\pi$ are probably associated with $M2\pi$, although they are not completely understood. Calculated line shapes for hot bands arising from first- and third-nearest-neighbor coupling, with the large negative exciton dispersion discussed above, are shown in Fig. 12. At 36°K, we expect no hot-band absorption from a single-magnon state to occur more than $51+74=125$ cm$^{-1}$ lower in energy than $M2\pi$. Hot bands $H2\sigma$ and $H2\pi$ appear to cut off at such an energy, but since we observe only the tails of these absorptions, their shape and intensity are difficult to estimate. $H2\pi$ peaks at about the correct place for a hot band arising from first-neighbor coupling, while the peak of $H2\sigma$ is not inconsistent with third-nearest-neighbor coupling. Thermal population of multimagnon states must be responsible for $H3\sigma$ and $H4\sigma$, but we do not presently understand the details of this absorption mechanism.

The slightly different stress behavior of the sidebands $E2\pi$ and $E2\pi a$ from that of their origin can be understood in terms of the first-nearest-neighbor coupling responsible for the large negative exciton dispersion. This is strongly dependent upon the $Mn^{+2}$-$Mn^{+2}$ distance along the $c$ axis. Compression along the [001] direction invariably reduces this distance and increases the coupling. Hence, as the crystal is compressed, $K_1$ increases and $E2\pi$ and $E2\pi a$ drop further below $M2\pi$ in energy. Using the known stress parameters[15] and assuming that the $Mn^{+2}$-$Mn^{+2}$ distances about an excited ion behave like those about a ground-state ion, we can determine the sensitivity of the exciton dispersion to distance. The ratio of the fractional change in $K_1$ to the fractional change of the $Mn^{+2}$-$Mn^{+2}$ distance is about 5.

$E2\pi a$ has been assigned as a bound exciton-magnon state,[36] the 1.6-cm$^{-1}$ separation from $E2\pi$ being the binding energy. This situation, in which a large negative exciton dispersion overcomes the positive magnon dispersion is most favorable for observing the bound state. Only in this circumstance will it appear at an energy where the unbound states do not absorb. Hence it cannot be masked or broadened by these other states. A theory describing such a state has been given recently by Freeman and Hopfield.[37]

The several weak absorptions to $^4A$ and $^4E$ occurring at higher energies are also of some interest. From Fig. 6 we see that three of these, $E3\pi$, $E5\pi$, and $E7\pi$, split in an 80-kG magnetic field like the magnetic dipole lines $M1\sigma$ and $M2\pi$.[34] $E3\pi$ is 98 cm$^{-1}$ above $M1\sigma$ and 83 cm$^{-1}$ above $M2\pi$. These energies are probably too low to be interpretable as odd-symmetry phonons. The Raman frequencies of $ZnF_2$ are similar to those of $MnF_2$.[38] This should be true of the IR-active modes as well. In $ZnF_2$ the three $E_u$ vibrations are observed[39] at 173, 294, and 380 cm$^{-1}$, whereas $A_{2u}$ occurs at 244 cm$^{-1}$. There are two $B_{1u}$ modes which are not IR-active, however.

Assuming that $E3\pi$ is neither a pure phonon sideband nor an impurity line, there remain two possibilities. The first is that it is a sideband to one of the $M_s=\mp\frac{1}{2}$ sublevels. Although $M_s$ is quite a good quantum number in this excited state, second-order spin-orbit coupling will give these substates a small amount of $M_s=\mp\frac{3}{2}$ character. Since $E3\pi$ is less intense than the identified magnon sidebands by at least three orders of magnitude, this is a possibility. The second alternative is that $E3\pi$ is a two-magnon sideband. Since this explanation presupposes a $\Delta M_s=\pm 1$ transition, spin-orbit coupling is necessary. This might take place, for instance, through the 0.1% quartet character of the ground state. The second magnon must be of even symmetry and can be excited on either sublattice with respect to the electronic excitation. Under either explanation $E3\pi$ is a weak magnon-assisted transition.

$E7\pi$ is about 50 cm$^{-1}$ above $E6\pi$. If $E6\pi$ is a zero-phonon sideband to the third $M_s=\mp\frac{3}{2}$ substate, then the same arguments apply to $E7\pi$ as to $E3\pi$. It is considerably higher in energy than $M1\sigma$ and $M2\pi$ and might also, therefore, be simply a phonon sideband. $E5\pi$ is

[36] R. S. Meltzer, Ming Y. Chen, M. Lowe-Pariseau, and D. S. McClure, Phys. Rev. Letters **21**, 913 (1968).
[37] S. Freeman and J. J. Hopfield, Phys. Rev. Letters **21**, 910 (1968).
[38] S. P. S. Porto, P. A. Fleury, and T. C. Damen, Phys. Rev. **154**, 522 (1967).
[39] M. Balkanski, P. Moch, and G. Parisot, J. Chem. Phys. **44**, 940 (1966).

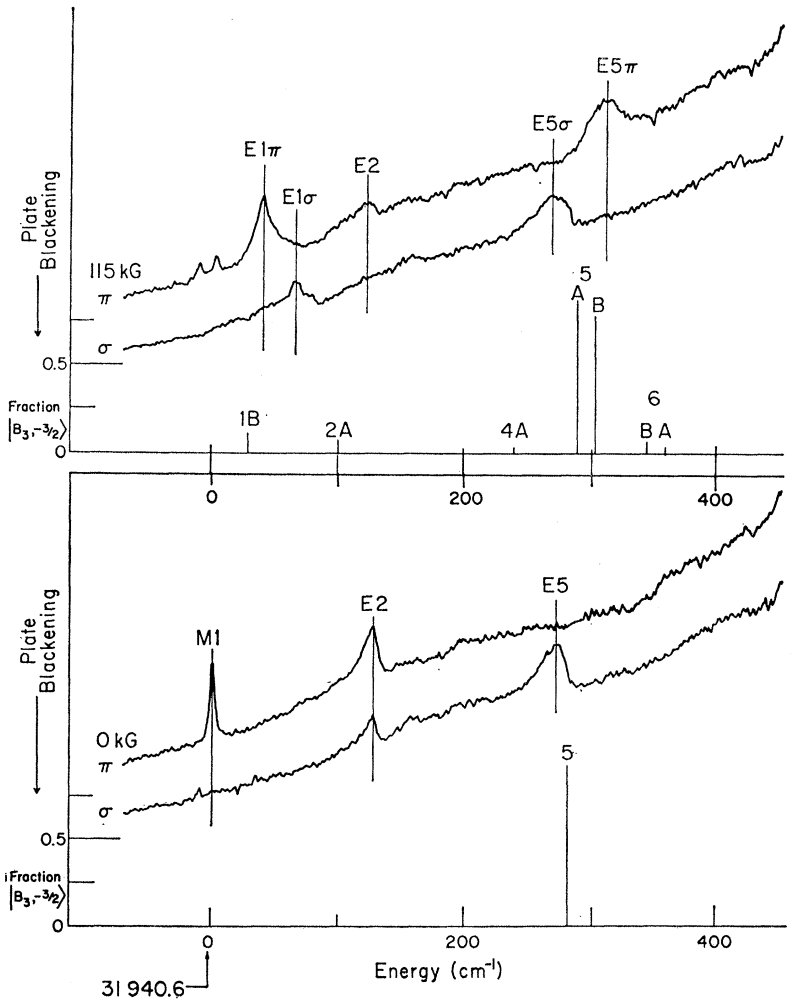


FIG. 13. Comparison of the ${}^6A_1 \rightarrow {}^4T_1$(II) absorption above and below, the flop field, at 4.2°K. The upper pair of curves show the absorption beyond the flop field at 115 kG, and the lower pair shows the absorption at 0 kG. The position of the vertical lines beneath the spectra indicates the energy; the height indicates the square of the coefficient of the $|B_3, -\frac{3}{2}\rangle$ substate in the solutions to the matrix of the ${}^4T_1$(II) state. The parameters of this calculation are described in the text.

150 $cm^{-1}$ above $M1\sigma$ or $M2\pi$ and may be a phonon sideband involving a low-energy odd-symmetry phonon.

$E4\pi$ is one or two orders of magnitude less intense than the no-phonon magnon sidebands. Although it may broaden somewhat in a magnetic field, it has a splitting factor considerably less than 2. It is therefore probably magnon-assisted.

It is clear that an explanation of these higher-energy transitions is a complicated matter, since there are several possible mechanisms with no present means of experimentally distinguishing some of them. However, many of these, on the basis of their magnetic field behavior and relative energy, appear to arise from magnon-assisted processes.

### D. ${}^4T_1$(II) State: 32 000 $cm^{-1}$

The low-energy region of the absorption to this cubic field state is shown in Fig. 13. The properties of the absorptions are summarized in Table II. The origin $M1\pi$ ($\Gamma_3^+$, $\Gamma_4^+$ exciton) is split by a magnetic field. The spectra above and below the flop-field magnetic transition are compared in the upper and lower sets of traces, respectively. A comparison reveals the appearance of several additional absorptions above the magnetic transition. We believe that these are spin-wave sidebands whose appearance can be explained in the following manner.

For the moment let us ignore the spin-orbit coupling and describe the single-ion basis states by the transformation properties of their orbital part under the site symmetry of $D_{2h}$, and by their spin projection. We have previously shown[15] for the ${}^4T_1$(II) cubic field state that its three orbital substates are ordered in energy $B_1 < B_3 < B_2$. The total energy spread is about 1000 $cm^{-1}$, with $B_3$ only 100 to 200 $cm^{-1}$ above $B_1$. Each orbital state is split by the exchange field into its four spin sublevels.

Let us suppose that excitons formed from $B_1$ orbital states do not couple to the magnons, whereas those formed from $B_3$ do. It follows that any sideband intensity accompanying a pure electronic transition must result from the presence of some $|B_3, \mp\frac{3}{2}\rangle$ character in that single-ion state. Spin-orbit coupling, which we have so far neglected, may mix the $B_1$ and $B_3$ states,

TABLE III. Pair moments associated with various magnon sidebands. The number given for the pair moment of each sideband is the square root of the sum of the squares of all the pair moments contributing to the sideband. In the cases where both $Z$ and $A$ points contribute, the number is the average given by the data. The symbols like $\pi_X^\pi$ are defined by Eqs. (9), (10), and the number given for the sideband moment is, e.g., $(\pi_X^\pi/64)^{1/2}$. The units are $10^{-4}$ D, where $D^2$ is 1 erg-cm$^3$.

| State | Electronic origin | Sidebands | | |
|---|---|---|---|---|
| $^4A, E$ | $M1\sigma$, $\Gamma_{1,2}$<br>$M2\pi$, $\Gamma_{3,4}$ | $E_{1\sigma}$ $\pi_{Z,A}^\sigma$ 6.5<br>$E_{2\sigma}$ $\pi_X^\sigma$ 11.3 | $E_{1\pi}$ $\pi_X^\pi$ 1.8<br>$E_{2\pi}$ $\pi_{Z,A}^\pi$ 4.3 | $H_{1\sigma}$ $\pi_1^\sigma$ 2.1 |
| $^4T_2$(II) | $M1\pi$, $\Gamma_{3,4}$ | $E_{1\sigma}$ $\pi_X^\sigma$ 4.7 | $E_{1\pi}$ $\pi_{Z,A}^\pi$ 2.7 | $H1\pi$ $\pi_1^\pi$ 2.7 |
| $^4T_1$(I) | $M1\sigma$, $\Gamma_{1,2}$<br>$M2\sigma$, $\Gamma_{1,2}$ | $E_{1\sigma}$ $\pi_{Z,A}^\sigma$ 1.4<br>$E_{2\sigma}$ $\pi_{Z,A}^\sigma$ 1.6 | $E_{1\pi}$ $\pi_X^\pi$ 1.2 | $H1\sigma$ $\pi_1^\sigma$ 2.1 |

but subject to the restriction that only excitons (formed from these single-ion states) of the same symmetry at the $\Gamma$ point of the zone are mixed.[40] Since the symmetry of the $|B_3, \mp\frac{3}{2}\rangle$ single-ion state is such that it may only occur in $\Gamma_1^+$, $\Gamma_2^+$ excitons, the lowest observed exciton may not have a sideband (which is $\Gamma_3^+$, $\Gamma_4^+$ if the lowest single-ion level is $|B_1, \mp\frac{3}{2}\rangle$). The second exchange field level of the $B_1$ state is, however, a $\Gamma_1^+$, $\Gamma_2^+$ exciton and may therefore borrow $|B_3, \mp\frac{3}{2}\rangle$ character via the spin-orbit coupling. The result is the sideband $E_2$, which, being composed predominantly of the $M_s=\mp\frac{1}{2}$ spin projection, can undergo a pseudosplitting in a magnetic field less than the flop field, as is observed.

When the flop field is exceeded, however, the magnetic space group is lowered. The two kinds of excitons may now be mixed. The exciton derived from the $|B_1, \mp\frac{3}{2}\rangle$ single-ion states can acquire $|B_3, \mp\frac{3}{2}\rangle$ character, and hence magnon sideband absorptions such as $E1\pi$ and $E1\sigma$ can occur. The height of the vertical lines beneath the microdensitometer traces of Fig. 13 indicates the square of the coefficient of the $|B_3, \mp\frac{3}{2}\rangle$ substate in that solution to the $12\times12$ matrix for the $^4T_1$(II) state.[41] Their positions indicate the eigenstate energy separations, where we have chosen the zero so that the energy of the first calculated eigenstate corresponds to that of a sideband to $M1\pi$, if it were observed. The agreement between the calculated and observed sideband intensities seems to confirm this model. It is therefore the details of the single-ion states which determine the strength of the coupled transitions.

The importance of the single-ion state in determining the sideband properties is also evident in Deitz's[4] strain results on the $^4T_1$(I) state. As [001] stress is applied, the orthorhombic ($D_{2h}$) orbital states separate in energy and are no longer mixed by the spin-orbit coupling. In the limit of large [001] stress, almost all the $\sigma$ sideband intensity appears associated with $B_2$ and the $\pi$ intensity with $B_3$. Under [110] stress the two substates $M1\sigma$ and $M2\sigma$ undergo an anticrossing, but the $\sigma$- and $\pi$-polarized sidebands follow the sublevels of $B_2$ and $B_3$ character, respectively.

### E. $^4E$(II) State: 30 000 cm$^{-1}$

Magnetic dipole transitions to the $^4E$(II) cubic field state are forbidden theoretically,[15] and have not been observed. One observes a hot band $H1\sigma$ about 90 cm$^{-1}$ lower in energy than a cold band appearing in both polarizations, $E1\pi$ and $E1\sigma$ (see Table II). Since these are electric dipole transitions and are unaffected by a magnetic field along the $c$ axis, we presume, by analogy with the other excited states, that these are magnon sidebands of the lowest orbital substate of $^4E$(II) having $M_s=\mp\frac{3}{2}$. The electric dipole absorption occurring 30 cm$^{-1}$ to the blue of $E1$ might be a sideband to the other orbital substate having $M_s=\mp\frac{3}{2}$. A 30-cm$^{-1}$ splitting of the $^4E$(II) state is consistent with the calculations of Goode,[42] in which the full $d^5$ matrix was diagonalized.

Assuming first-nearest-neighbor coupling for the hot band, its polarization indicates that the lowest exciton is $\Gamma_1^+$, $\Gamma_2^+$. Since $E1\pi$ is 5 cm$^{-1}$ lower in energy than $E1\sigma$, we assume the exciton dispersion of the lowest exciton to be relatively small. The second orbital substate with $M_s=\mp\frac{3}{2}$ must then give rise to a $\Gamma_3^+$, $\Gamma_4^+$ exciton. The relative positions of $E2\sigma$ and $E2\pi$ are also consistent with a small exciton dispersion.

## V. CONCLUSIONS

Let us now return to the four questions with which we began. It appears that the existing theory for magnon sideband absorption is basically satisfactory in that the combined exciton-magnon dispersion, obtained from the sum of the exciton and magnon dispersions, describes the main features of both the cold bands and hot bands. Its shortcomings appear most evident in absorption to $^4T_1$(I), the only state studied in detail prior to this work. Exciton-magnon interactions have recently been suggested as the main difficulty,[33] but even the hot band to this state, for which such an explanation does not

[40] In considering the sidebands we must really consider the symmetry of the critical points in the dentsiy of states. However, compatibility tables show that the two kinds of excitons give rise to different irreducible representations at the critical points. See, for instance, J. O. Dimmock and R. G. Wheeler, Phys. Rev. **127**, 391 (1962).

[41] In order to fit the over-all data best, the energy difference of $B_3$ and $B_1$ was increased to 220 cm$^{-1}$ and the spin-orbit coupling increased by a factor of 1.6 compared to Ref. 15. These changes do not alter any conclusions of Ref. 15.

[42] D. H. Goode, J. Chem. Phys. **43**, 2830 (1965).

TABLE IV. Vibrational overlap factors, magnon induced intensity, and exciton dispersion. Columns 2 and 3 represent two ways to get the vibrational overlap factor. $F(M)$ taken from Ref. 15 is the ratio of observed to calculated magnetic dipole oscillator strength. Column 4 is the oscillator strength of the identified magnon sidebands of each state. Column 5 gives the exciton dispersion parameter. Column 6 is the fraction of intensity induced by magnons, corrected for vibrational overlap using $F(M)$.

| State | Fraction $t_2^3e^2$ | $F(M)=\frac{f_{obs}(M)}{f_{calc}(M)}$ | $f_{obs}(C)\times10^9$ | $K_1$ ($cm^{-1}$) | $\frac{f_{obs}(C)}{f_{obs}(E)F(M)}$ |
|---|---|---|---|---|---|
| $^4A_4E$(I) | 1.00 | 1.2 | 269 | 2.0 ($M1\sigma$)<br>37.0 ($M2\pi$) | 0.50 |
| $^4T_2$(II) | 0.83 | 0.71 | 28 | 6.65 | 0.18 |
| $^4T_1$(II) | 0.45 | 0.20 | 2.65 | ··· | 0.02 |
| $^4T_1$(I) | 0.01 | 0.04 | 3.9 | 0 ($M1\sigma$)<br>0 ($M2\sigma$) | 0.25 |

apply, appears anomalously broad, suggesting the importance of phonon-magnon interactions. With regard to each of the other excited states, however, both hot-band and cold-band absorption peaks can be fitted rather well with one set of exciton dispersion parameters.

The intensity of the cold bands may be understood simply in terms of second-nearest-neighbor intersublattice coupling, whereas for the hot bands, both this and first-nearest-neighbor intrasublattice coupling appear important. We find no evidence of absorption intensity arising from third-neighbor coupling other than possibly the hot band $H2\sigma$ of the $^4A$, $^4E$ state, which indicates the short-range nature of the intensity producing exchange mechanism. In $MnF_2$, the pair moments responsible for coupled absorption appear to be of the same order of magnitude for second- (intersublattice) as for first- (intrasublattice) nearest-neighbor exciton-magnon coupling (see Table III).

The exciton dispersion in these excited states appears to vary considerably. In $M1\sigma$ of the $^4T_1$(I) state it is less than 1 $cm^{-1}$, whereas for $M2\pi$ of the $^4A_1$, $^4E$(I) states it is about 75 $cm^{-1}$. The dispersion arises predominantly from exchange interaction between nearest-neighbor $Mn^{+2}$ ions (along the $c$ axis) and is predominantly negative. (See Table IV.)

Except for the sidebands of $M1\sigma$ of the $^4T_1$(I) state, exciton-magnon interactions appear to be no larger in energy than a few $cm^{-1}$. In absorption to the $^4A_1$, $^4E$(I) states we observe what is probably a small exciton-magnon interaction in the form of a bound exciton-magnon state. If this is true, the interaction in this state is 1.6 $cm^{-1}$.

Although there are several possible kinds of magnon-assisted and phonon-assisted transitions in magnetic crystals, some of which are difficult to distinguish experimentally, it is true that any electric dipole process in $MnF_2$ which is not split by a magnetic field must involve a magnon. In such a case the transition derives its intensity from magnon-exciton coupling. Hence a major portion of the absorption to the $^4T_2$(II) and $^4A_1$, $^4E$(I) state has been shown to be magnon-assisted, and this is probably true of the entire spectrum of $MnF_2$.

We have seen that we may set an upper limit to the contribution of phonon-assisted processes (see Sec. II C). These results are summarized in columns 3–5 of Table IV. Column 6 gives the minimum fraction of magnon contribution to the intensity. The difference between this and unity is presumably the maximum fraction of the phonon contribution.

It should be emphasized that the numbers in column 6 are probably much smaller than the actual fraction of magnon contribution. In both the $^4T_2$(II) and $^4T_1$(II) states, $f_{obs}(C)$ includes sidebands to only one orthorhombic state, since only these are clearly identifiable. This is true especially with regard to the $^4T_1$(II) state, since the lowest orthorhombic state appears to have associated with it very little sideband intensity. In the $^4T_1$(I) state we have included sidebands to two of three orthorhombic substates. Only in the case of $^4A_1$, $^4E$(I) have we included all three orbital components. In any case, it is clear that magnon-assisted processes make an important contribution to the total electric dipole intensity.

Finally, we must attempt to understand, in a general way, the differences and similarities between the excitons and their magnon sidebands in the several excited states. Some of their properties are summarized in Table IV. We have chosen to order the states in the table such that the following properties are in decreasing order: column 2, the fraction of $t_2^3e^2$ character; column 3, the ratio of observed to calculated magnetic dipole intensity $F(M)$ (see Ref. 15, Table I); column 4, the oscillator strengths $f(C)$ of the magnon sidebands; and column 5, the exciton dispersion $K_1$. It is no accident that these four properties change in the same way from state to state.

The connection between the excited-state fraction of $t_2^3e^2$ character and the ratio of the calculated to observed oscillator strength for the magnetic dipole transitions stems from the importance of the vibrational overlap between the ground and excited states. The vibrational overlap is dependent upon the electronic similarity of the ground and excited states. Since the ground state is almost exclusively $t_2^3e^2$, the extent to which the excited state consists of this configuration is a measure of the

vibrational overlap. The oscillator strengths for the magnetic dipole transitions have the form

$$f^q(MD) \propto |\langle e_{01}{}^q|\mathbf{m}|g_{01}{}^0\rangle|^2 \propto |\langle\psi_{01}(e)|\mathbf{m}|\psi_{01}(g)\rangle \times\langle\phi_{01}{}^q(e)|\phi_{01}{}^0(g)\rangle|^2 \propto S^2(0,q), \quad (17)$$

where $\psi$ and $\phi$ are the electronic and vibrational wave functions which we have separated in accordance with the Born-Oppenheimer approximation. The two subscripts refer to the ion and sublattice, respectively, on which the excitation resides. The superscripts refer to the vibrational excitation. The intensity of the zero-phonon lines is proportional to the square of the (0,0) overlap. (See column 3, Table IV.)

Now consider the matrix elements which give rise to the intersublattice exchange coupling responsible for the temperature-independent magnon sidebands. They have the form

$$f^q(C) \propto (\langle e_{01}{}^q m_{n2}{}^0|\mathbf{P}_{\rm eff}|g_{01}{}^0 g_{n2}{}^0\rangle)^2 \propto [\langle\psi_{01}(e)\psi_{n2}(m)|\mathbf{P}_{\rm eff}|\psi_{01}(g)\psi_{n2}(g)\rangle \times\langle\phi_{01}{}^q(e)|\phi_{01}{}^0(g)\rangle\langle\phi_{n2}{}^0(m)|\phi_{n2}{}^0(g)\rangle]^2 \propto S^2(0,q), \quad (18)$$

where $\mathbf{P}_{\rm eff}$ is the effective electric dipole moment operator. The electronic wavefunction of the magnon, however, is simply that of the ground state. Hence the second overlap integral is unity and the intensity of the zero-phonon sideband is also proportional to the square of the (0,0) vibrational overlap of the ground and excited electronic states. This is also true of the hot band, as can easily be verified. (See column 4, Table IV.)

The exciton dispersion, however, also depends upon this overlap, since

$$K_1 \propto \langle e_{01}{}^0 g_{n1}{}^0|V_{01,n1}|g_{01}{}^0 e_{n1}{}^0\rangle \propto \langle\psi_{01}(e)\psi_{n1}(g)|V_{01,n1}|\psi_{01}(g)\psi_{n1}(e)\rangle \times\langle\phi_{01}{}^0(e)|\phi_{01}{}^0(g)\rangle\langle\phi_{n1}{}^0(g)|\phi_{n1}{}^0(e)\rangle \propto S^2(0,0), \quad (19)$$

where $V_{01,n1}$ is the electron exchange operator for ions 0 and $n$. In this case, the two vibrational overlap integrals are identical and equal to the (0,0) vibrational overlap. Hence $K_1$ is also proportional to $S^2(0,0)$. This explains, for instance, as has been noted by Dietz and Misetich,[33] the negligible exciton dispersion in the $^4T_1$(I) state, for which the vibrational overlap is about 0.1. (See column 6, Table IV.)

There are, of course, other particulars upon which the magnon sideband intensity and exciton dispersion depend, but since the vibrational overlaps differ appreciably in the several excited states, a general correlation of these properties to the similarity in the electronic wave functions of the ground and excited states is of basic importance.

With regard to vibronic states, the vibrational overlap with the ground state, and therefore the exciton dispersion, may be very different from that of the zero-phonon states. As a result, the magnon-assisted intensity, which appears in the Franck-Condon distribution, may have line shapes very different from the zero-phonon sidebands which act as the origin. If the exciton dispersion is large, this may lead to broadening of the magnon-assisted intensity appearing in the Franck-Condon distribution. This is, of course, in addition to effects of the phonon dispersion. These multiple excitations are therefore extremely complicated.

We have found that the vibrational overlap between the ground and excited states is of basic importance in understanding absorption in $MnF_2$. It is essential in understanding the single-ion electronic states which serve as an interpretation of the magnetic dipole spectrum and in understanding the differences and similarities in that part of the spectrum which results from coupling between the ions. Although $MnF_2$ is an ideal case for study, these conclusions presumably apply to a host of other magnetic crystals in which coupling between the optically active ion and its environment is large.

## ACKNOWLEDGMENTS

We would like to express our thanks to Professor J. W. Stout, whose assistance in this work was indispensable. In particular, we are indebted to him for most of the $MnF_2$ samples, for permission to use Figs. 4 and 8 from his unpublished file of spectra, and for a great deal of good advice. We also thank Philip G. Russell for permission to use some of his unpublished high-magnetic-field data on $MnF_2$. We are grateful to R. E. Dietz and H. J. Guggenheim for providing several samples of $MnF_2$, and to Dr. Dietz for some valuable discussions.